Available online at www.CivileJournal.org

Civil Engineering Journal

(E-ISSN: 2476-3055; ISSN: 2676-6957)

Vol. 10, No. 12, December, 2024

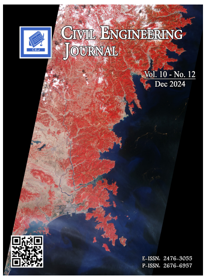

Analysis of Climate Change Scenarios Using the LARS-WG 8 Model Based on Precipitation and Temperature Trends

Saad H. Hadi [1*], Husam H. Alwan [1], Fadhil M. Al-Mohammed [2]

[1] *Department of Civil Engineering, College of Engineering, University of Kerbala, Kerbala 56001, Iraq.*

[2] *Al-Furat Al-Awsat Technical University, Kerbala 56001, Iraq.*

Received 06 August 2024; Revised 15 November 2024; Accepted 21 November 2024; Published 01 December 2024

Abstract

Global food production and water distribution are at risk due to increasing temperatures and changing precipitation trends. The main objective of the study was to analyze the climate trend and future projections in seven stations in southern Iraq. The period (1981–2020) was designated as a base period. The periods (2021-2040) and (2041-2060) were defined as the future two periods. The Mann-Kendall trend test was employed to assess trends utilizing XLSTAT. The study employed the most recent version of the LARS-WG 8 model to forecast climate change by using three GCMs (ACCES-ESM1-5, HadGEM3-GC31-LL, and MRI-ESM2-0). These simulations are based on two scenarios (SSP-245 and SSP-585). The statistical indicators provided support for the outcomes of model calibration and validation, demonstrating its competence and reliability. The results of this analysis indicate that there is a non-significant increase in precipitation and a considerable increase in both maximum and minimum temperatures during the period (1981-2060). The downscaled result reveals an increase in monsoon precipitation in the range of 2.233-2.831 mm under SSP-245 and SSP-585, respectively, compared with the base periods 1981-2020 during the Near Future and 1.988-2.543 mm during the mid-future. Also, annual maximum/minimum temperature increases in the range of (1.156-1.549 °C) and (1.486-1.770 °C) during the Near Future. (2.095-2.892 °C) and (1.486-1.770 °C) during the mid-future, respectively, for SSP-245 and SSP-585. These outcomes can enhance understanding to develop strategies for mitigating and adapting to these impacts.

Keywords: Climate Change; GCM Models; LARS-WG 8; Mann-Kendall Test; Precipitation; Southern Iraq; Temperatures.

1. Introduction

Climate change is a global phenomenon characterized by three significant indicators: (1) a progressive increase in global average temperatures, (2) alterations in global precipitation patterns, and (3) rising sea levels [1]. The rise in atmospheric carbon dioxide, with other greenhouse gases and anthropogenic activities such as land use alterations and industrial effluent production, contributes to alterations in both global and regional climates [2]. Iraq is facing significant and interconnected environmental, security, economic, and political challenges, and climate change is likely to intensify these issues. Elevated temperatures, reduced precipitation, extreme drought, desertification, salinization, and heightened dust storms have adversely impacted Iraq's agriculture. Iraq's water security is contingent upon the Tigris and Euphrates rivers, which have experienced diminished water levels. Political instability at national and regional levels obstructs efforts to combat climate change, which will affect Iraq in the forthcoming years [3]. A 2018 assessment by the Expert Working Group on Climate-Related Security Risks indicates that climate change has resulted in extended heat waves, unpredictable rainfall, elevated temperatures, and heightened catastrophe intensity in Iraq. As water levels decline, the rising salinity of water sources has emerged as a significant issue in southern Iraq, particularly in Basra [4]. On the

* Corresponding author: saad.h@s.uokerbala.edu.iq

http://dx.doi.org/10.28991/CEJ-2024-010-12-014

agricultural front, Iraq's drought years became particularly severe in 2018, when the country's cultivated land was cut in half. Rice production lost $39 million following the government's cessation of irrigated agricultural cultivation, including maize and other grains [5]. In 2019, Iraq represented 8% of global methane emissions and 0.5% of worldwide carbon dioxide emissions. Its per capita greenhouse gas emissions surpass the global average (see Figure 1) [6, 7].

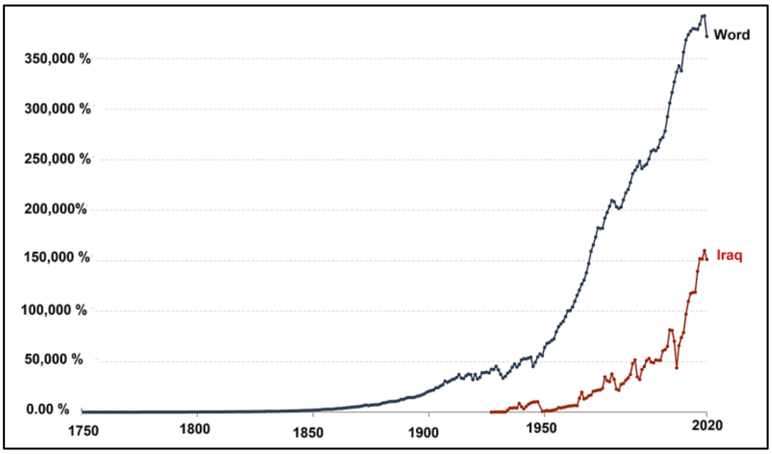

Figure 1. Shows change in annual CO_2 emissions [7]

The Intergovernmental Panel on Climate Change (IPCC) has unequivocally shown human activities, especially the emission of greenhouse gases, are the primary drivers of global warming. The Earth's surface temperature rose by 1.1ºC between 2011 and 2020 compared to the average temperature documented from 1850 to 1900. In 2021, Iraq encountered its most acute drought in four decades, but Syria faced its most extreme drought in seven decades. The temperature rose by 0.2 °C (0.36 °F) from 1961 to 1990, and the 2021 IPCC study corroborated earlier evaluations indicating that the Middle East and Mediterranean nations would face heightened droughts and wildfires. Regional temperatures are anticipated to increase by a minimum of 2 °C (3.6 °F) or more by the middle of the century [8-10]. In March 2023, the IPCC released its yearly report, revealing that climate change presents a substantial hazard to 3.3 to 3.6 billion individuals globally, subjecting them to heightened risk of life-threatening occurrences [11]. According to the International Monetary Fund (IMF), climatic disasters in the region have resulted in an average of $2 billion in direct material damages annually and have impacted more than seven million residents annually [12].

In this study, Numerical models (General Circulation Models, or GCMs) were used. The (GCMs) are dependable and influential models that faithfully simulate the physical processes in the atmosphere, land surface, and ocean. Their role is essential in predicting future climate change in response to the rising release of greenhouse gases [13]. However, the GCMs typically have a horizontal resolution that spans from 250 to 600 km; this level of precision needs to be revised to satisfy the spatial resolution requirements of several local impact studies [14].

The studies conducted by Semenov & Barrow (2002) [15] and Wilby et al. (2007) [16] have shown that statistical downscaling models are a cost-effective and efficient method for examining the exact effects of climate change on specific localized locations. The Long Ashton Research Station Weather Generator (LARS WG) model is widely employed for simulating climate variables in current and future scenarios [17-19]. Multiple experiments conducted in Iraq have repeatedly verified the appropriateness and practicality of the LARS-WG model in different areas of the nation, covering a diverse set of climate conditions under CMIP3 and CMIP5 [20-23]. The (IPCC) implemented CMIP6 as part of the sixth Assessment Report (AR6). Unlike CMIP5, which solely took into account Representative Concentration Pathways (RCPs), CMIP6 presents a novel scenario framework that integrates Shared Socioeconomic Pathways (SSPs) with Representative Concentration Pathways (RCPs) [25-27].

A study by Muhaisen et al. (2024) [21] in Northern Iraq assessed the efficacy of LARS-WG 6 in performing a downscaling analysis. The study aims to generate prospective daily meteorological data and climate change projections for the Mosul Dam Reservoir. The results indicated that minimum and maximum temperatures (Tmin and Tmax) exhibited the most substantial increases of (+5.7 °C) in July and (+5.3 °C) in September, respectively, from 2081 to 2100 under the RCP8.5 scenario. Similarly, Mukheef et al. (2024) [20] employed LARS-WG 6 in Iraq's Middle and West regions to forecast climatic change. The results of this study indicate that the temperature and rainfall patterns under two future scenarios for the period from 2023 to 2050 exhibit a rising tendency when compared to the observed patterns from 1983 to 2014. The predictions indicate that there will be a rise in annual maximum temperatures by the end of this century, ranging (+1.26 ◦C to + 2.08 ◦C) for SSP-245 and (+1.57 ◦C to + 2.34 ◦C) for SSP-585 at all study locations. The analysis revealed the yearly rise in rainfall (+3.56% to +3.87%) for SSP-245 and (+7.22% to +12.61%) for SSP-585. Mohamed and Hassan (2022) [27] projected that the mean annual Tmin and Tmax for all locations (southern Iraq) from 2021 to 2100 under the RCP4.5 and RCP8.5 scenarios would increase by (+1.41 to +1.50) °C and (+5.67 to +5.91) °C, respectively. The GCM HadGEM2-ES model predicted a more substantial increase in temperature under both scenarios relative to the other models. The projected reduction in rainfall by the five GCMs demonstrates diverse trends across all locations from 2021 to 2100. The CanESM2 model forecasted the most substantial rise in rainfall (29.9 mm) under RCP8.5, while the MIROC5 model suggested the largest potential decline in rainfall (6.4 mm). Hassan et al. (2022) [28] demonstrated that the average annual (Tmin and Tmax) across all sites in central and western Iraq will rise by (+0.94 to 4.98) °C by the end of the 21st century. According to historical data from 1990 to 2020, the annual variations in rainfall for the study area are projected to rise by (6.09% to 14.31%) under RCP4.5 and (11.25% to 20.97%) under RCP8.5.

Despite continuous research, uncertainties remain regarding the expected long-term air temperature and precipitation changes under future climate scenarios [29]. The lands of southern Iraq are vital for agricultural operations and are essential to ensuring food security for the region. They significantly contribute to the country's total grain production [30]. The projections of climate variables, such as rainfall and air temperature, are highly significant since they profoundly impact monthly and seasonal fluctuations and variations. These parameters significantly influence important features such as the timing of planting, the duration of growth, and the scheduling of irrigation [31]. The objective of this study is to evaluate the baseline trend of average monthly precipitation using the traditional trend analysis method. Furthermore, this study aims to forecast alterations in rainfall and atmospheric temperatures in Southern Iraq, specifically under the recently constructed Shared Socioeconomic Pathways (SSPs) such as SSP-245 and SSP-585. The timeframes considered are the near-term (2021-2040) and the midterm (2041-2060). To achieve this, widely acknowledged statistical downscaling models, such as LARS-WG 8, will be employed. Furthermore, the study assessed the ability of individual (GCMs) integrated into the most recent version of LARS-WG 8 to downscale and compared their performance to multi-model ensembles.

This study is crucial for water resource and agricultural management, providing valuable insights into anticipated climate variability under future climate scenarios. This is especially crucial for susceptible places and might substantially influence the overall food security throughout the nation.

2. Material and Methods

2.1. Study Area

The study stations are situated in southern Iraq. The geographic coordinates of these places span from latitude 29° 6' 23" to 32° 46' 40" N and longitude 43° 9' 00" to 47° 7' 39" E (see Figure 2). The southern region of Iraq is a crucial agricultural center, well-known for its vital contribution to producing grain, cotton, and fruit. Nevertheless, the study area often encounters difficulties with desertification and limited water resources, resulting in substantial financial damages in the agricultural and industrial sectors [32]. The southern parts of Iraq consist predominantly of alluvial plains and arid basins. The main soil types consist of silt and clay, which contain tiny and fine particles measuring less than 0.07 mm in diameter. These particles are susceptible to being lifted and carried by the wind with considerable ease. Due to the scarcity of flora, these particles are easily exposed to the wind and prone to becoming airborne [33]. This renders the study region susceptible to dust storms [34]. The climate is mainly continental, subtropical, and semi-arid. It is hot, with an average temperature exceeding 45°C during July and August and decreasing to 25°C at night [34, 36]. This region is characterized by its low annual rainfall, which is at most 200 mm per year. For this reason, small dams were constructed in the valleys of the Western Desert to harvest water during the rainy seasons and use it in summer [35]. Rainfall occurs during winter, specifically from December to February [37].

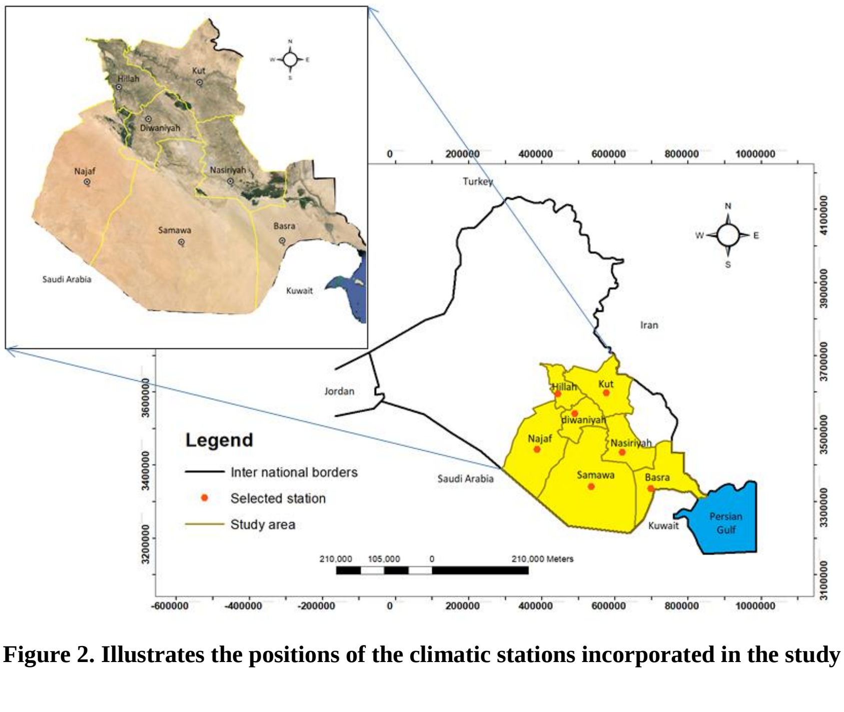

Figure 2. Illustrates the positions of the climatic stations incorporated in the study

2.2. Data

Rainfall, Tmax, and Tmin are required for trend analysis and running of the LARS-WG model. This study utilized seven stations to examine the rainfall and temperature, as outlined in (Table 1).

Table 1. Geospatial data regarding the precise whereabouts of the seven chosen stations within the designated study region

Station name	Lat.	Long.	Elevation (a.s.l.)	Length of record	Location
Diwaniyah	32.00º	44.01º	21	1981- 2020	Iraq
Samawa	30.19º	45.38º	8	1981- 2020	Iraq
Najaf	31.12º	43.82º	60	1981- 2020	Iraq
Nasiriyah	31.04º	46.26º	9	1981- 2020	Iraq
Hillah	32.49º	44.42º	34	1981- 2020	Iraq
Kut	32.51º	45.82º	20	1981- 2020	Iraq
Basra	30.13º	47.08º	5	1981- 2020	Iraq

The currently accessible rain gauges do not offer complete daily data, often containing gaps in the information. Consequently, researchers typically rely on another source of rainfall data. The present research utilizes CHIRPS to obtain daily rainfall data for all seven study locations. NASA Power also offers daily, time-varying Tmax and Tmin for global energy resources. These data, obtained from the website *https://power.larc.nasa.gov/data-access-viewer*, were utilized in the current study for seven climatic stations. The weather generator model underwent calibration and validation utilizing daily climate data from 1981 to 2020.

Figure 3 displays the structural framework of this investigation, specifically the input/output interactions. The diagram illustrates the sequential process to be undertaken in this investigation. Figure 4 shows the average monthly rainfall and temperature data for the reference period (1981 to 2020). Figure 5 shows that the climate of the study area is desert or dry, symbolized by the symbol (B W h) according to the Köppen classification.

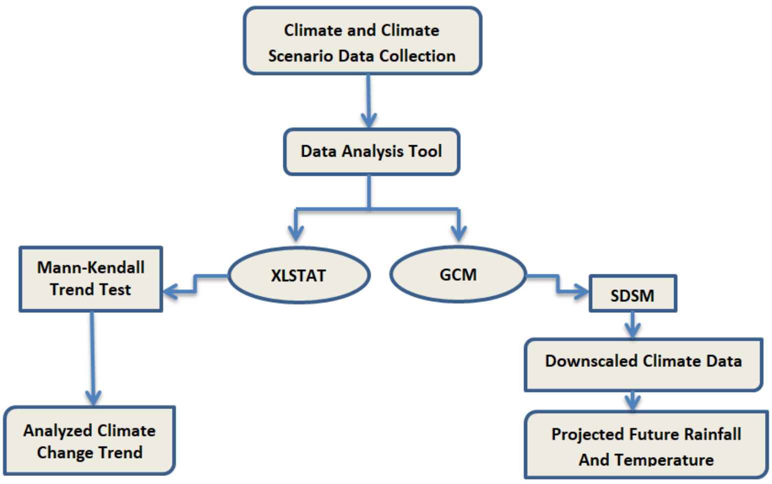

Figure 3. Displays the structural framework of this study

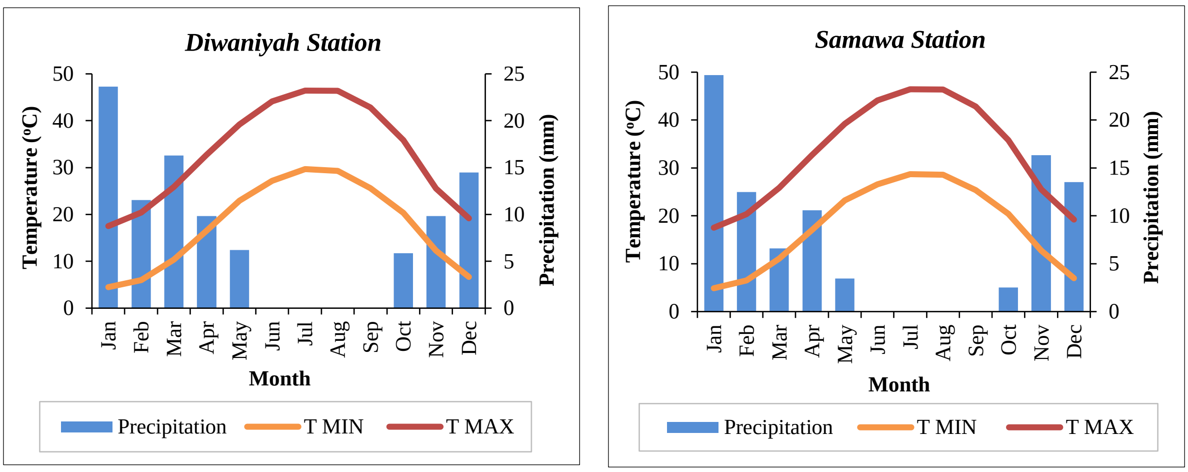

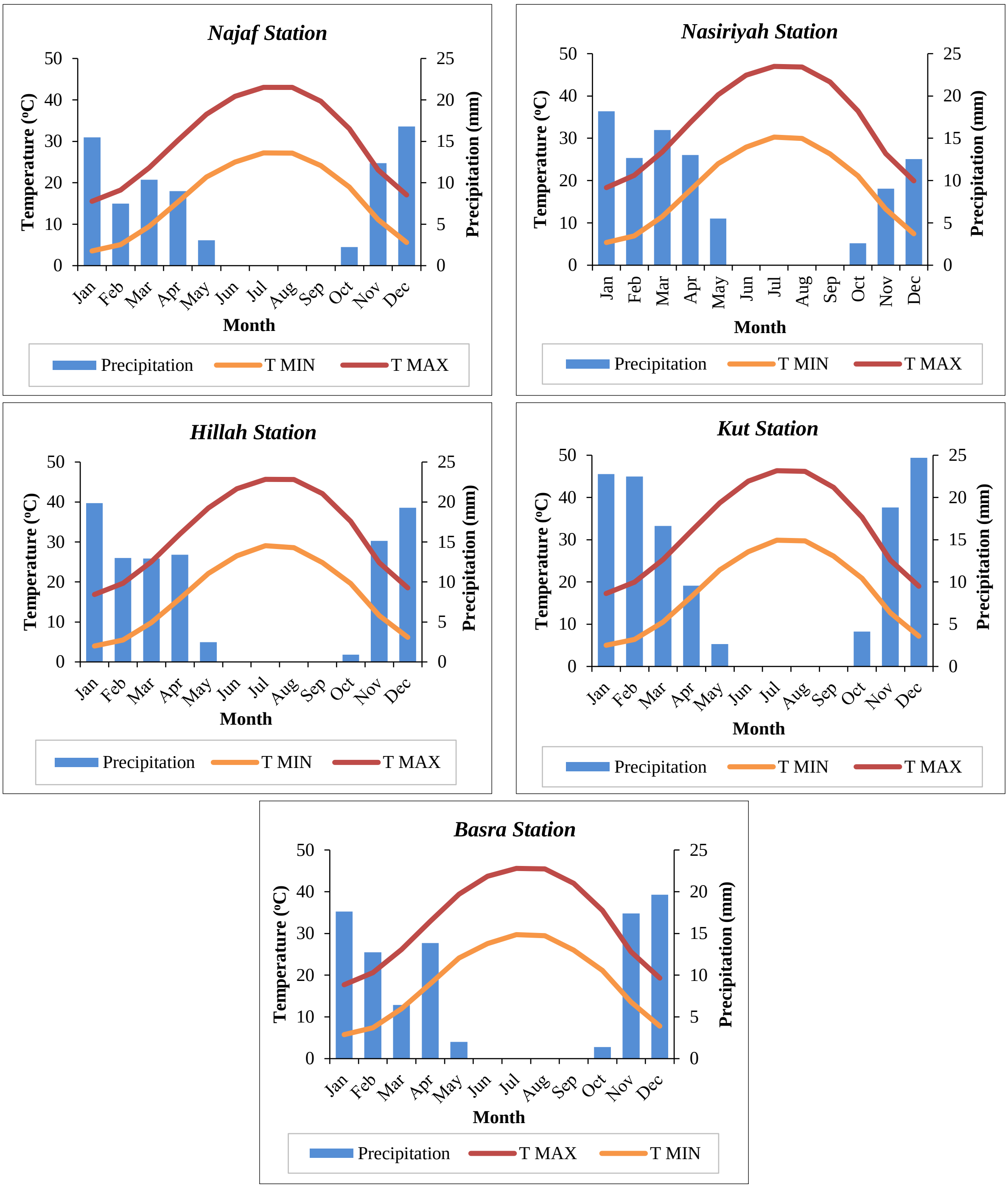

Figure 4. Average monthly Tmax, Tmin and Precipitation for baseline period (1981–2020)

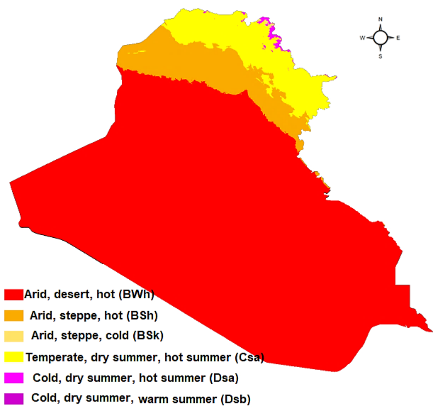

Figure 5. Köppen–Geiger climate classification map for Iraq (2071-2100) [38]

The Köppen climate classification is based on precipitation and temperature. It was invented by the German-Russian climatologist Vladimir Peter Köppen in 1900 by combining the 1866 world vegetation map and the five-zone climate division map of Alfonso Piram de Candolle. Study area within A desert climate, or arid climate, is a climate that is only part of the polar climate in that its precipitation is very poorly tolerated, except for some plants that can tolerate such a harsh climate. It is symbolized in the Köppen climate classification by BWh, BWk, and sometimes BWn. Such areas usually receive rainfall ranging from 25 to 200 mm per year, and in some years, they may not receive any precipitation at all. These areas are considered to have a desert climate due to the high degree of evaporation, as they lose more water than they gain [38].

Figures 4 and 6 indicate that Al-Kut station recorded the highest monthly precipitation rate, whereas Najaf station registered the lowest monthly precipitation rate over 40 years (1981 to 2020). All stations lacked precipitation during June, July, August, and September. Nasiriyah and Basra stations registered the highest monthly average temperatures, unlike Najaf station, which recorded the lowest monthly average.

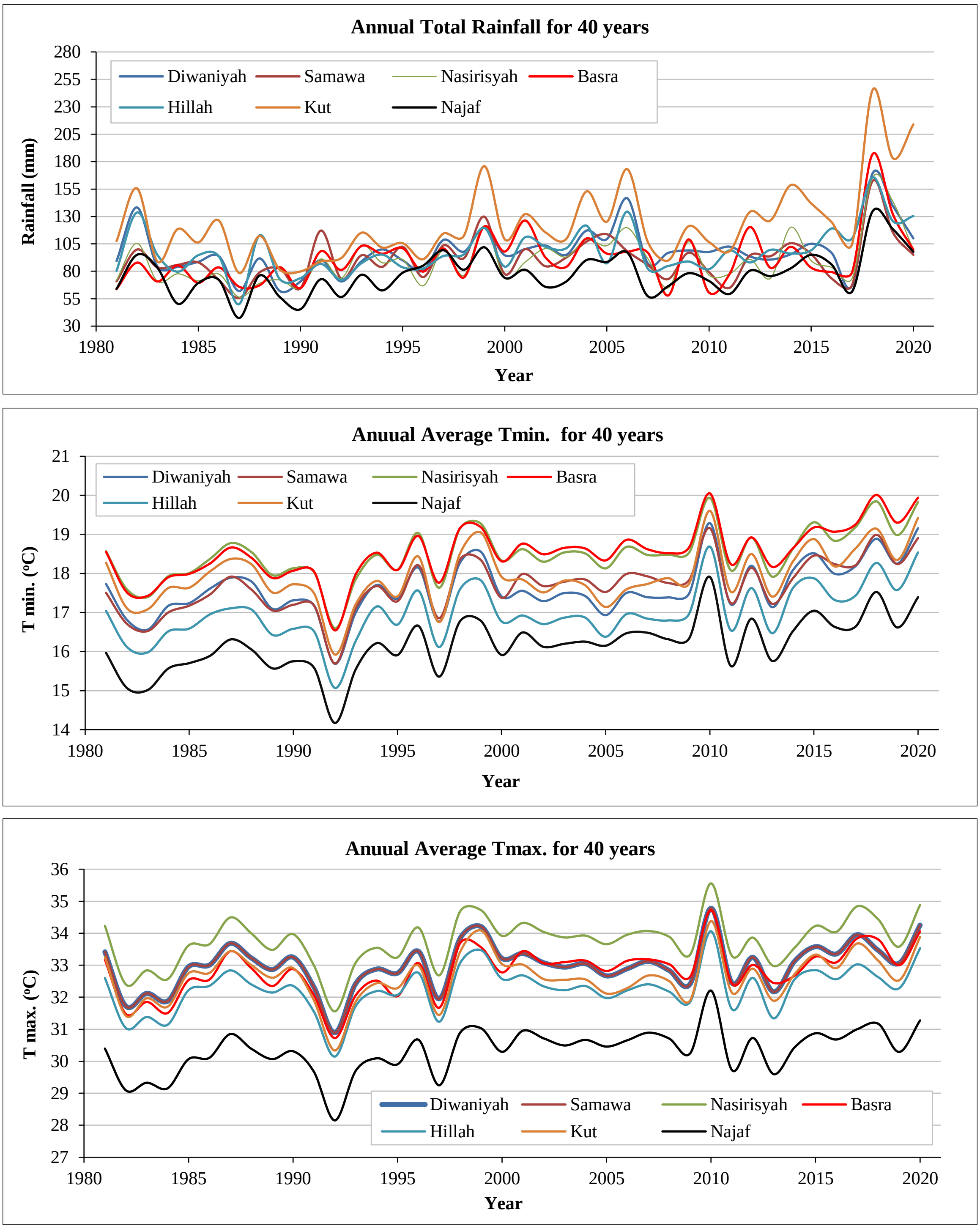

Figure 6. Mean annual Rainfall, Tmin, and Tmax of the study area (1981–2020)

2.3. Trend Analysis

An essential area of research before projecting future climatic variables is analyzing trends in meteorological variables because climate change continues to affect various aspects of life [39, 40]. Assessing climate change effects in a particular region typically depends on examining crucial meteorological factors, such as rainfall and atmospheric temperature [41].

In recent years, other techniques have been employed to identify patterns in hydro-meteorological parameters, such as the Mann-Kendall (MK) test [42, 43] and Sen's slope method [44]. The current study employed these methodologies to analyze and assess the trend of monthly average rainfall and temperature.

2.3.1. Mann- Kendall Trend Analysis

The (MK) test is extensively utilized for examining trends in hydrological, meteorological, and climatic data. The current study used the MK test to identify the historical rainfall pattern in southern Iraq using long-term data from 1981 to 2020. The statistic S was computed using Equation 1 [42, 43, 45]:

$$S = \sum_{i=1}^{n-1} \sum_{j=n+1}^{n} sgn(y_j - y_i) \tag{1}$$

where (S) represent the MK test statistic, (n) denotes the number of data points, and (y_i) and (y_j) signify annual values for years j and i, where j > i. The function $sgn(y_j - y_i)$ assumes the following values: $sgn(y_j - y_i) =$

$$\begin{matrix} 1, & if \ (y_j - y_i) > 0 \\ 0, & if \ (y_j - y_i) = 0 \\ -1, & if \ (y_j - y_i) < 0 \end{matrix} \tag{2}$$

Suppose (y_i) and (y_j) are independent and randomly ordered, and there are at least ten data series ($n \geq 10$). In that case, the MK statistic is distributed according to a normal distribution with an expected value E(S) = 0. Equation 3 is used to determine the variance Var (S), whereas Equation 4 is used to calculate (Z- statistic).

$$Var(S) = \frac{n(n-1)(2n+5)}{18} \tag{3}$$

$$Z = \begin{cases} \frac{s-1}{\sqrt{v_s}} & for\ S > 0 \\ 0 & for\ S = 0 \\ \frac{s+1}{\sqrt{v_s}} & for\ S < 0 \end{cases} \tag{4}$$

where (n) is number of tied (zero difference between compared values), Z is the standard normal distribution (Z – statistics).

Statistically, The Z-value evaluates a trend's importance. A (+Z) value signifies an upward trend, whereas a (- Z) value denotes a downward trend.

MAKESENS uses a two-tailed test at four significance levels (α = 0.1, 0.05, 0.01, and 0.001). A significance level of 0.001 denotes a 0.1% probability that the values xi arise from a random distribution, reflecting the chance of incorrectly rejecting the null hypothesis (H_0) of no trend. A significance level of 0.001 denotes a substantial likelihood of a monotonic trend's presence. A significance criterion 0.1 denotes a 10% likelihood of incorrectly rejecting (H_0). This study presented trends at a significance level of α = 0.05 and used a 95% confidence level for the standard normal statistic (Z) to evaluate the trends in sequence variation.

2.3.2. Sen's Slope Estimator

Sen (1968) [44] proposed a statistical technique called the famous slope, which measures the rate of change over time. The present study utilized the Sen slope estimator to determine the yearly variation in rainfall patterns in southern Iraq. For a detailed description of the calculation of Sen's slope estimator, see the study of He & Gautam (2016) [46].

The subsequent equation is employed to calculate each slope (Qi):

$$Q_i = \frac{Y_j - Y_i}{j-1}, \qquad j > i \tag{5}$$

Yj and Yi represent the data values at times j and i, respectively, and (i) changes from 1 to n-1 and (j) from 2 to n. In a time series with n values of Yj, the slope estimates will be N = (n(n-2)/2). The slope of the Sen estimator is the average slope of the N values of those slopes. Sen's slope denotes a statistical technique employed to ascertain the slope of a trend line within time series data.

$$Q_{ij} = \begin{cases} \frac{Yj-Yi}{J-1} & if\ n\ is\ odd \\ \frac{1}{2}\left[Q\ \frac{N}{2} + Q\left(\frac{N+2}{2}\right)\right] & if\ n\ is\ even \end{cases} \tag{6}$$

where the positive (Q_i) indicates an ascending trajectory, whilst the negative (Q_i) values suggest a downward trend in the temporal data, and the unit of Sen's slope (Q_i) represents the slope's annual magnitude.

2.4. Projected Climate Data for the Future

Once the baseline precipitation trends have been analyzed, the next step is to forecast future changes in climate elements using (GCMs) based on different climate scenarios.

The LARS-WG is a computational tool for generating synthetic time series of meteorological conditions that exhibit statistical similarities to observed data [15]. The most recent iteration of LARS-WG 8 has successfully incorporated the most up-to-date (CMIP6) multi-model ensemble, which was utilized in the latest IPCC AR6. In contrast to LARS-WG 6, which scenarios (RCP-2.6, RCP-4.5, and RCP-8.5) alongside eighteen GCMs from the CMIP5. The most recent version (LARS-WG8) integrates three Shared Socioeconomic Pathways (SSP-126, SSP-245, and SSP-585) with three (GCMs) from the (CMIP6) [47]. Table 2 presents the descriptions of the three (GCMs) incorporated into the most recent iteration of LARS-WG 8.

Table 2. A detailed description of the (GCMs) is included in the current version of LARS-WG 8

GCMs	Institute / country	Resolution (Lon. × Lat.)
ACCES – ESM 1- 5	CSIRO / Australia	1.9° × 1.2°
HadGEM3- GC31- LL	Met Office / UK	1.8° × 1.2°
MRI-ESM 2 - 0	MRI / Japan	1.1° × 1.1°

This study used three CMIP6 General Circulation Models (GCMs) to analyze the period from 1983 to 2020. Using a collection of climate models from CMIP6, an analysis has been conducted on the variations in temperature and precipitation. This analysis focuses on present and future conditions, considering two future scenarios. The SSP-245 is characterized as a moderate emission scenario, whereas SSP-585 indicates a high greenhouse gas emission setting, indicating a period with minimal efforts to alleviate the impacts of climate change [48]. The estimation of climate change was conducted for two specific future periods: the first period, which is near (2021-2040), and the second period, which is an intermediate timeframe (2041-2060).

2.4.1. Evaluating the Performance of LARS-WG

The present study utilized a sequence of statistical tests to adjust and confirm the model's accuracy. The Kolmogorov-Smirnov (K-S) statistical test was used to evaluate the degree of similarity between the daily rainfall distributions in simulated and real data, as well as the wet/dry series' seasonal distributions. Furthermore, it assesses the dispersion of daily rainfall and the daily lowest and highest temperatures. This test offers a statistical metric that determines whether to accept or reject the hypothesis that the two datasets may come from the same distribution. A low p-value and a high KS value suggest that the simulated data is highly unlikely to be similar to the genuine data. Therefore, it is not recommended to use the data for model evaluation. The researchers Semenov & Barrow (2002) [15] advocated using a p-value of 0.01 as the accepted limit for the model's results. A p-value of 0.05 is generally regarded as a sufficient significance level in most statistical analyses.

Ideal fit match is established when the p-value equals 1. A p-value < 1 and p-value ≥ 0.7 indicates a very good. A good is indicated by a p-value < 0.7 and p-value ≥ 0.4, whereas a poor is indicated by a p-value < 0.4. The difference between simulated and observed data can emerge from various factors, including the application of smoothing to observed data, random fluctuations, and inaccuracies in the original data. Statistical indicators were used for the goodness-of-fit test of the model created by LARSWG8 when simulating observed and generated data in the calibration and validation phases.

Three statistical parameters will be employed to assess the LARS-WG 8: (R^2), (NSE) index, and (RMSE) to the standard deviation of observed data (STDobs) (RSR). These statistical factors are utilized to compare the simulated outcomes with the actual results of the observed data. The range of R^2 values is zero to one, and a higher value indicates greater model performance. (N_{SE}) value of zero or higher indicates that the simulated value is more accurate in predicting the concerned component than the average observed value. Conversely, an N_{SE} value of one means the achievement of optimal modeling. The N_{SE} assesses the discrepancy between the observed and predicted data by comparing it with a best-fit line exhibiting a 1:1 ratio.

The (RMSE) ratio to the observed data's standard deviation is used to evaluate errors. Therefore, a simulation is considered appropriate if (RSR) < 0.5; see the study conducted by Moriasi et al. [49].

The following equations are used to derive the statistical parameters:

$$R^2 = \frac{\sum_1^n P_i O_i}{\sqrt{\sum_1^n P_i^2 \sum O_i^2}} \tag{7}$$

$$N_{SE} = 1 - \frac{\sum_{i=1}^n (Pi - Oi)^2}{\sum_{i=1}^n (Pi - Oa)^2} \tag{8}$$

$$RSR = \frac{RMSE}{STD_{ob}} = \frac{\sqrt{\sum_{i=1}^n (Pi - Oi)^2}}{\sum_{i=1}^n (Pi - Oa)^2} \tag{9}$$

where (Pi) indicates the estimated daily value for climatic variables, (Oi) signifies the actual daily value, (n) indicates the total number of data points utilized, and (Oa) represents the average of observed data values.

3. Results and Discussion

3.1. Calibration and Validation Results for Lars-WG

The model was calibrated and validated using daily data from seven locations in southern Iraq from 1981 to 2020. The statistical test results are presented in Table 3, which displays the observed seasonal data, and Table 4, which shows the simulated daily rainfall for each month.

Table 3. The (K-S) test is used to analyze the distributions of the seasonal wet / dry series

Season	Wet / dry	N	K-S	P-Value	Assessment
Diwaniyah Station					
DJF	wet	11.50	0.033	1.000	Ideal fit
DJF	dry	11.50	0.059	1.000	Ideal fit
MAM	wet	11.50	0.026	1.000	Ideal fit
MAM	dry	11.50	0.07	1.000	Ideal fit
JJA	wet	11.50	0.304	0.196	Poor
JJA	dry	11.50	0.087	1.000	Ideal fit
SON	wet	11.50	0.018	1.000	Ideal fit
SON	dry	11.50	0.147	0.949	Very good
Kut Station					
DJF	wet	11.50	0.035	1.000	Ideal fit
DJF	dry	11.50	0.059	1.000	Ideal fit
MAM	wet	11.50	0.019	1.000	Ideal fit
MAM	dry	11.50	0.126	0.988	Very good
JJA	wet	11.50	0	1.000	Ideal fit
JJA	dry	11.50	0.348	0.096	Poor
SON	wet	11.50	0.02	1.000	Ideal fit
SON	dry	11.50	0.046	1.000	Ideal fit
Nasiriyah Station					
DJF	wet	11.50	0.032	1.000	Ideal fit
DJF	dry	11.50	0.058	1.000	Ideal fit
MAM	wet	11.50	0.037	1.000	Ideal fit
MAM	dry	11.50	0.099	1.000	Perfect
JJA	wet	11.50	0.435	0.017	Poor
JJA	dry	11.50	0.218	0.589	Good
SON	wet	11.50	0.046	1.000	Ideal fit
SON	dry	11.50	0.081	1.000	Ideal fit
Basra Station					
DJF	wet	11.50	0.025	1.000	Ideal fit
DJF	dry	11.50	0.078	1.000	Ideal fit
MAM	wet	11.50	0.015	1.000	Ideal fit
MAM	dry	11.50	0.074	1.000	Ideal fit
JJA	wet	11.50	0	1.000	Ideal fit
JJA	dry	11.50	0.217	0.595	Good
SON	wet	11.50	0.043	1.000	Ideal fit
SON	dry	11.50	0.073	1.000	Ideal fit

Season	Wet/dry	N	K-S	P-Value	Assessment
Hillah Station					
DJF	wet	11.50	0.045	1.000	Ideal fit
DJF	dry	11.50	0.055	1.000	Ideal fit
MAM	wet	11.50	0.075	1.000	Ideal fit
MAM	dry	11.50	0.067	1.000	Ideal fit
JJA	wet	11.50	0	1.000	Ideal fit
JJA	dry	11.50	0.478	0.006	Poor
SON	wet	11.50	0.026	1.000	Ideal fit
SON	dry	11.50	0.104	0.999	Very good
Najaf Station					
DJF	wet	11.50	0.028	1.000	Ideal fit
DJF	dry	11.50	0.062	1.000	Ideal fit
MAM	wet	11.50	0.037	1.000	Ideal fit
MAM	dry	11.50	0.114	0.997	Very good
JJA	wet	11.50	0.435	0.017	Poor
JJA	dry	11.50	0.044	1.000	Ideal fit
SON	wet	11.50	0.06	1.000	Ideal fit
SON	dry	11.50	0.115	0.996	Very good
Samawa Station					
DJF	wet	11.50	0.039	1.000	Ideal fit
DJF	dry	11.50	0.105	0.999	Very good
MAM	wet	11.50	0.017	1.000	Ideal fit
MAM	dry	11.5	0.13	0.984	Very good
JJA	wet	11.5	0	1.000	Ideal fit
JJA	dry	11.5	0.261	0.359	Poor
SON	wet	11.5	0.02	1.000	Ideal fit
SON	dry	11.5	0.077	1.000	Ideal fit

Table 4. The results of (K-S) test for the distributions of daily precipitation

Month	N	K-S	P-Value	Assessment	Month	N	K-S	P-Value	Assessment
Diwaniyah Station					**Hillah Station**				
J	11.50	0.065	1.000	Ideal fit	J	11.50	0.130	0.984	Very good
F	11.50	0.135	0.976	Very good	F	11.50	0.134	0.978	Very good
M	11.50	0.132	0.981	Very good	M	11.50	0.184	0.789	Very good
A	11.50	0.044	1.000	Ideal fit	A	11.50	0.174	0.842	Very good
M	11.50	0.051	1.000	Ideal fit	M	11.50	0.381	0.052	Poor
J	11.50	0.609	0.000	Poor	J	11.50	0.000	1.000	Ideal fit
J	No rainfall		-	Poor	J	No rainfall		-	Poor
A	No rainfall		-	Poor	A	No rainfall		-	Poor
S	No rainfall		-	Poor	S	No rainfall		-	Poor
O	11.50	0.095	1.000	Ideal fit	O	11.50	0.057	1.000	Ideal fit
N	11.50	0.117	0.995	Very good	N	11.50	0.117	0.995	Very good
D	11.50	0.122	0.992	Very good	D	11.50	0.065	1.000	Ideal fit
Kut Station					**Najaf Station**				
J	11.50	0.065	1.000	Ideal fit	J	11.50	0.127	0.987	Very good
F	11.50	0.065	1.000	Ideal fit	F	11.50	0.129	0.985	Very good
M	11.50	0.130	0.984	Very good	M	11.50	0.069	1.000	Ideal fit
A	11.50	0.103	0.999	Very good	A	11.50	0.231	0.514	Good
M	11.50	0.337	0.115	Poor	M	11.50	0.172	0.851	Very good
J	11.50	0.478	0.006	Poor	J	11.50	0.609	0.000	Poor
J	No rainfall		-	Poor	J	No rainfall		-	Poor
A	No rainfall		-	Poor	A	11.50	1.000	0.000	Poor
S	11.50	0.870	0.000	Poor	S	11.50	1.000	0.000	Poor
O	11.50	0.184	0.789	Very good	O	11.50	0.202	0.685	Good
N	11.50	0.070	1.000	Ideal fit	N	11.50	0.129	0.985	Very good
D	11.50	0.065	1.000	Ideal fit	D	11.50	0.261	0.359	Poor
Nasiriyah Station					**Samawa Station**				
J	11.50	0.069	1.000	Ideal fit	J	11.50	0.065	1.000	Ideal fit
F	11.50	0.073	1.000	Ideal fit	F	11.50	0.129	0.985	Very good
M	11.50	0.066	1.000	Ideal fit	M	11.50	0.075	1.000	Ideal fit
A	11.50	0.082	1.000	Ideal fit	A	11.50	0.137	0.972	Very good
M	11.50	0.109	0.998	Very good	M	11.50	0.078	1.000	Ideal fit
J	11.50	0.609	0.000	Poor	J	11.50	1.000	0.000	Poor
J	No rainfall		-	Poor	J	No rainfall		-	Poor
A	No rainfall		-	Poor	A	11.50	1.000	0.000	Poor
S	11.50	1.000	0.000	Poor	S	11.50	1.000	0.000	Poor
O	11.50	0.170	0.861	Very good	O	11.50	0.144	0.957	Very good
N	11.50	0.173	0.847	Very good	N	11.50	0.070	1.000	Ideal fit
D	11.50	0.065	1.000	Ideal fit	D	11.50	0.130	0.984	Very good
Basra Station									
J	11.50	0.121	0.993	Very good					
F	11.50	0.064	1.000	Ideal fit					
M	11.50	0.101	1.000	Ideal fit					
A	11.50	0.093	1.000	Ideal fit					
M	11.50	0.255	0.388	Poor					
J	11.50	0.739	0.000	Poor					
J	11.50	1.000	0.000	Poor					
A	No rainfall		-	Poor					
S	11.50	0.609	0.000	Poor					
O	11.50	0.221	0.572	good					
N	11.50	0.065	1.000	Ideal fit					
D	11.50	0.130	0.984	Very good					

Table 3 displays the statistical analysis results of the seasonal data collected during the validation phase. Table 4 illustrates the efficacy of daily precipitation models for each month. The symbol (N) represents the number of tests conducted in each table. In Table 3, the model yields satisfactory outcomes when assessing wet and dry series distributions. The performance was either exemplary or highly satisfactory at all stations during the winter (DJF) and autumn (SON) seasons. The spring season evaluation (MAM) demonstrated high accuracy (perfect fit). At the same time, throughout the summer (JJA), the model exhibited poor performance in several areas throughout the dry and wet seasons, indicating overall poor performance. The poor performance in distributing dry interval series during the dry season is attributed to the absence or scarcity of rainfall, which hinders the model's ability to accurately account for dry spells and assess the weather conditions.

The assessments in Table 4 demonstrate that the model's performance in simulating daily rain distributions is excellent in all months except for summer, which is consistent with the explanation provided earlier. When comparing the observed data with simulated data for the average monthly Tmax, Tmin, and rainfall for all stations, Table 5 shows the results of (R^2), (NSE), and (RSR). The statistical indicators revealed a robust association between the observed data and the downscaled data from the model. The (R^2) demonstrated a robust association across the three climatic variables, varying from 0.851 to 0.999. Simultaneously, the mean bias error (MBE) and root mean square error (RSR) values ranged from 0.387 to 0.982 and from 0.003 to 0.055, respectively, for the climatic variables.

Table 5. presents the statistical parameter values for the baseline period of 1981 to 2020, obtained from the calibration and validation of the LARS-WG model

Scenarios		SSP-245						SSP-585					
Period		2021-2041			2041-2060			2021-2041			2041-2060		
Performance Indicators		R^2	N_{SE}	RSR	R^2	N_{SE}	RSR	R^2	N_{SE}	RSR	R^2	N_{SE}	RSR
Diwaniyah station	Precip.	0.901	0.664	0.023	0.931	0.823	0.017	0.944	0.792	0.018	0.954	0.795	0.018
	T min	0.998	0.971	0.056	0.997	0.936	0.008	0.977	0.958	0.007	0.996	0.881	0.011
	T max	0.999	0.987	0.003	0.998	0.957	0.006	0.999	0.976	0.004	0.996	0.922	0.008
Hillah station	Precip.	0.958	0.709	0.020	0.933	0.819	0.016	0.897	0.387	0.029	0.974	0.826	0.015
	T min	0.998	0.971	0.006	0.997	0.934	0.008	0.997	0.958	0.007	0.995	0.881	0.011
	T max	0.999	0.987	0.003	0.998	0.955	0.006	0.998	0.975	0.004	0.998	0.923	0.008
Kut station	Precip.	0.949	0.893	0.010	0.971	0.846	0.012	0.963	0.660	0.017	0.950	0.893	0.010
	T min	0.998	0.970	0.006	0.997	0.935	0.008	0.996	0.958	0.007	0.994	0.870	0.012
	T max	0.998	0.986	0.003	0.999	0.958	0.006	0.998	0.977	0.004	0.996	0.921	0.008
Najaf station	Precip.	0.898	0.684	0.027	0.957	0.776	0.023	0.896	0.562	0.032	0.964	0.756	0.024
	T min	0.998	0.968	0.006	0.997	0.924	0.009	0.997	0.953	0.007	0.995	0.869	0.012
	T max	0.999	0.985	0.004	0.998	0.954	0.006	0.998	0.973	0.005	0.998	0.911	0.009
Nasiriyah station	Precip.	0.913	0.705	0.024	0.958	0.884	0.015	0.963	0.717	0.023	0.942	0.458	0.032
	T min	0.998	0.969	0.006	0.997	0.934	0.008	0.997	0.956	0.007	0.996	0.868	0.012
	T max	0.999	0.986	0.003	0.998	0.957	0.006	0.998	0.976	0.004	0.998	0.920	0.008
Samawa station	Precip.	0.890	-0.054	0.039	0.920	0.119	0.035	0.864	-0.830	0.050	0.851	-1.18	0.055
	T min	0.997	0.955	0.007	0.996	0.925	0.009	0.997	0.953	0.007	0.995	0.862	0.013
	T max	0.998	0.976	0.004	0.998	0.958	0.006	0.998	0.975	0.004	0.997	0.921	0.008
Basra station	Precip.	0.942	0.880	0.013	0.984	0.960	0.008	0.958	0.801	0.017	0.948	0.749	0.019
	T min	0.998	0.970	0.006	0.997	0.932	0.009	0.997	0.959	0.007	0.996	0.868	0.012
	T max	0.998	0.984	0.004	0.998	0.956	0.006	0.998	0.973	0.005	0.997	0.916	0.008

The model is highly effective in precisely forecasting minimum and maximum temperatures and precipitation, verifying that it applies to all sites for the present study. The three GCMs were chosen based on the calibration of the average results (Table 6). The findings indicated that all three models are congruent with the local context of the study area since their applicability to other locations necessitates verification by the KS test for distributions of seasonal wet and dry series. The models exhibited satisfactory performance in the humid region. In contrast to the two models (ACCESS- ESM1-5 and HadGEM3- GC31-LL), performance in hyper-arid and arid areas, particularly during the summer season (JJA), is suboptimal.

Table 6. shows a fit of three GCM models to the study area using (the KS-test) for wet/dry season series distributions

Seasonal	Wet/Dry	Effective n	ACCESS - ESM1- 5		Had GEM3 - GC31- LL		MRI – ESM 2 - 0	
			KS	P-value	KS	P- value	KS	P-value
DJF	wet	11.500	0.041	1.000	0.027	1.000	0.029	1.000
DJF	dry	11.500	0.072	1.000	0.056	1.000	0.062	1.000
MAM	wet	11.500	0.109	0.872	0.060	0.997	0.033	1.000
MAM	dry	11.500	0.099	0.996	0.062	1.000	0.108	0.997
JJA	wet	11.500	0.076	0.957	0.000	0.750	0.120	0.858
JJA	dry	**11.500**	**0.294**	**0.379**	**0.381**	**0.049**	**0.174**	**0.815**
SON	wet	11.500	0.055	0.996	0.046	0.997	0.136	0.753
SON	dry	11.500	0.093	0.998	0.118	0.974	0.085	0.999

The p-value is computed to determine whether to accept or reject the hypothesis that the two data sets derive from the same distribution, namely that the observed climatic values correspond with the simulated values. A low p-value and a high KS value indicate that the simulated climate is improbable to align with the observed climate; hence, it should be rejected (Table 6).

3.2. MK and Sen’s Slope Test

Climate change trend analysis is crucial for drought monitoring. The non-parametric (MK) test is the prevailing method for detecting climate change patterns in time series data [42, 43]. The (M K) trend test was employed to examine rainfall and temperature data trends. The (MK) trend tests were conducted using XLSTAT. The experiments were performed with a significance level of 5% for seven southern Iraq stations. The trend changes were classified into four categories: significant increasing trend ($p \leq \alpha$, Z^{+}), significant decreasing trend ($p \leq \alpha$, Z^{-}), non-increasing trend ($p > \alpha$, Z^{+}) and non-decreasing trend ($p > \alpha$, Z^{-}) [50]. Based on the Z statistics and p-values, the MK trend test noted that there was a non-increasing trend in rainfall for all stations in different seasons, except for the Diwaniyah and Samawa stations, which differed in the presence of a significantly increasing trend for the summer season (JJA). When analyzing the Tmin, a significant increasing trend was observed at all stations for the summer season (JJA). In contrast, the other seasons showed a non-insignificant increasing trend. The trend was observed at Basra station for the two seasons: the summer (JJA) and spring (MAM), Najaf station showed a notable increasing tendency exclusively during the summer season (JJA), unlike the other stations, which displayed a non-significant increasing trend. Table 7 provides the Z statistic, the p-value of the (MK) test, and (Sen's slope) value for all stations.

Table 7. Estimated values Sen’s Slope and Kendall’s test statistics for all seasons from 1981 to 2020

Variable	Minimum	Maximum	Mean	Std. deviation	S	Var.(S)	Alpha(α)	p-value	Sen's slope	Z_c
Diwaniyah: Rainfall										
DJF	4.647	42.990	16.727	9.172	60.667	7366.667	0.050	0.511	0.070	0.700
MAM	2.227	22.390	10.774	4.426	-24.667	7366.667	0.050	0.369	0.011	-0.287
JJA	0.000	0.117	0.003	0.018	13.000	7366.667	0.050	**0.033**	0.000	0.147
SON	0.000	24.467	5.231	4.583	68.333	7366.667	0.050	0.161	0.031	0.790
Diwaniyah: Max. Temperature										
DJF	15.364	23.997	19.082	1.809	62.000	7366.667	0.050	0.525	0.019	0.713
MAM	28.578	35.915	32.607	1.589	44.667	7366.667	0.050	0.254	0.016	0.517
JJA	43.123	48.171	45.648	1.214	176.667	7366.667	0.050	0.084	0.031	2.050
SON	29.438	37.835	34.650	1.623	64.000	7366.667	0.050	0.300	0.012	0.740
Diwaniyah: Min. Temperature										
DJF	2.176	10.625	5.745	1.863	63.333	7366.667	0.050	0.526	0.021	0.727
MAM	13.673	19.313	16.621	1.310	102.000	7366.667	0.050	0.379	0.023	1.187
JJA	26.212	31.075	28.711	1.119	294.667	7366.667	0.050	**0.002**	0.050	3.423
SON	16.540	22.252	19.391	1.399	162.667	7366.667	0.050	0.248	0.035	1.883
Samawa: Rainfall										
DJF	5.598	43.062	17.077	8.717	-21.000	7366.667	0.050	0.433	-0.045	-0.237
MAM	1.548	18.636	6.873	3.930	138.000	7366.667	0.050	0.149	0.066	1.597
JJA	0.000	0.138	0.009	0.033	32.667	7366.667	0.050	0.210	0.000	0.373
SON	1.915	25.003	6.283	4.441	58.667	7366.667	0.050	0.386	0.029	0.680

Samawa: Max. Temperature										
DJF	15.364	23.997	19.082	1.809	62.000	7366.667	0.050	0.525	0.019	0.713
MAM	28.578	35.915	32.607	1.589	44.667	7366.667	0.050	0.254	0.016	0.517
JJA	43.123	48.171	45.648	1.214	176.667	7366.667	0.050	0.084	0.031	2.050
SON	29.438	37.835	34.650	1.623	64.000	7366.667	0.050	0.300	0.012	0.740
Samawa: Min. Temperature										
DJF	2.411	10.732	6.165	1.839	86.000	7366.667	0.050	0.348	0.027	0.990
MAM	14.181	19.897	17.109	1.278	150.000	7366.667	0.050	0.084	0.037	1.947
JJA	25.268	30.396	27.952	1.162	309.667	7366.667	0.050	**0.002**	0.054	3.597
SON	16.547	22.113	19.498	1.303	160.000	7366.667	0.050	0.291	0.035	1.853
Nasiriyah: Rainfall										
DJF	3.604	37.729	14.549	8.394	60.333	7366.667	0.050	0.531	0.064	0.690
MAM	2.090	28.207	11.505	6.495	113.000	7366.667	0.050	0.346	0.078	1.313
JJA	0.000	0.120	0.009	0.032	30.333	7366.667	0.050	0.150	0.000	0.347
SON	0.000	19.181	3.877	3.904	48.333	7366.667	0.050	0.309	0.022	0.560
Nasiriyah: Max. Temperature										
DJF	16.103	25.017	19.895	1.916	62.000	7366.667	0.050	0.523	0.022	0.713
MAM	29.403	37.153	33.568	1.651	69.333	7366.667	0.050	0.249	0.024	0.803
JJA	43.737	48.635	46.259	1.146	183.333	7366.667	0.050	0.074	0.031	2.123
SON	30.205	38.378	35.294	1.571	60.000	7366.667	0.050	0.235	0.011	0.693
Nasiriyah: Min. Temperature										
DJF	2.923	11.622	6.632	1.889	48.000	7366.667	0.050	0.630	0.018	0.547
MAM	14.494	20.609	17.732	1.287	147.333	7366.667	0.050	0.205	0.029	1.703
JJA	26.848	31.579	29.374	1.105	310.667	7366.667	0.050	**0.002**	0.052	3.607
SON	17.425	22.855	20.217	1.307	147.333	7366.667	0.050	0.335	0.030	1.717
Basra: Rainfall										
DJF	4.161	52.810	16.876	9.663	48.000	7366.667	0.050	0.581	0.067	0.553
MAM	1.000	19.014	7.437	4.144	186.000	7366.667	0.050	0.156	0.091	2.157
JJA	0.000	0.087	0.005	0.019	24.000	7366.667	0.050	0.442	0.000	0.270
SON	0.000	30.487	6.262	5.594	51.000	7366.667	0.050	0.240	0.031	0.590
Basra: Max. Temperature										
DJF	15.497	24.362	19.248	1.928	118.000	7366.667	0.050	0.225	0.034	1.363
MAM	29.252	36.275	32.821	1.536	134.000	7366.667	0.050	0.332	0.034	1.547
JJA	42.335	47.284	44.913	1.131	208.000	7366.667	0.050	**0.038**	0.038	2.413
SON	29.380	37.250	34.293	1.493	83.000	7366.667	0.050	0.224	0.015	0.963
Basra: Min. Temperature										
DJF	3.295	11.746	7.042	1.846	88.000	7366.667	0.050	0.351	0.028	1.013
MAM	15.054	20.781	17.996	1.257	190.000	7366.667	0.050	**0.050**	0.038	2.200
JJA	26.373	31.173	28.905	1.099	351.667	7366.667	0.050	**0.000**	0.058	4.083
SON	17.337	22.842	20.215	1.259	168.000	7366.667	0.050	0.335	0.032	1.947
Hillah: Rainfall										
DJF	4.472	44.268	17.663	8.828	42.000	7366.667	0.050	0.636	0.057	0.473
MAM	1.869	22.590	9.603	4.703	48.667	7366.667	0.050	0.628	0.059	0.563
JJA	0.000	0.101	0.005	0.020	2.667	7366.667	0.050	0.858	0.000	0.027
SON	0.000	22.521	5.357	4.017	76.333	7366.667	0.050	0.236	0.032	0.880
Hillah: Max. Temperature										
DJF	14.665	23.263	18.394	1.810	59.333	7366.667	0.050	0.538	0.021	0.683
MAM	27.988	35.109	31.829	1.569	34.000	7366.667	0.050	0.343	0.015	0.393
JJA	42.206	47.553	44.877	1.286	158.000	7366.667	0.050	0.122	0.032	1.830
SON	28.664	37.165	33.956	1.634	77.667	7366.667	0.050	0.455	0.017	0.900

Hillah: Min. Temperature										
DJF	1.566	10.032	5.242	1.864	76.000	7366.667	0.050	0.476	0.023	0.873
MAM	13.095	18.476	15.920	1.282	86.000	7366.667	0.050	0.463	0.023	0.990
JJA	25.534	30.477	28.073	1.103	306.667	7366.667	0.050	**0.002**	0.050	3.563
SON	15.823	21.579	18.687	1.430	178.000	7366.667	0.050	0.166	0.040	2.060
Kut: Rainfall										
DJF	7.591	63.606	23.763	13.050	107.333	7366.667	0.050	0.330	0.164	1.240
MAM	2.018	24.011	9.611	4.857	92.667	7366.667	0.050	0.345	0.046	1.073
JJA	0.000	0.105	0.006	0.021	14.333	7366.667	0.050	0.169	0.000	0.167
SON	0.000	32.865	7.661	6.538	85.667	7366.667	0.050	0.179	0.094	0.997
Kut: Max. Temperature										
DJF	14.858	23.658	18.780	1.855	50.000	7366.667	0.050	0.475	0.017	0.577
MAM	27.847	35.592	32.057	1.714	14.667	7366.667	0.050	0.341	0.008	0.167
JJA	43.056	47.827	45.464	1.156	153.333	7366.667	0.050	0.107	0.027	1.777
SON	29.217	37.457	34.230	1.656	54.667	7366.667	0.050	0.362	0.011	0.633
Kut: Min. Temperature										
DJF	2.491	10.914	6.230	1.884	58.667	7366.667	0.050	0.567	0.019	0.670
MAM	13.397	19.587	16.645	1.413	62.000	7366.667	0.050	0.365	0.012	0.720
JJA	26.421	31.210	28.929	1.145	234.333	7366.667	0.050	**0.018**	0.045	2.717
SON	17.183	22.836	19.902	1.392	151.333	7366.667	0.050	0.307	0.031	1.753
Najaf: Rainfall										
DJF	2.036	35.100	13.453	7.371	41.000	7366.667	0.050	0.647	0.028	0.467
MAM	0.000	16.438	7.475	3.788	67.667	7366.667	0.050	0.515	0.045	0.773
JJA	0.000	0.139	0.006	0.026	34.000	7366.667	0.050	0.133	0.000	0.390
SON	0.000	23.263	4.871	4.132	56.333	7366.667	0.050	0.401	0.046	0.653
Najaf: Max. Temperature										
DJF	13.338	21.879	17.008	1.825	74.667	7366.667	0.050	0.349	0.027	0.870
MAM	26.487	33.421	30.118	1.536	80.667	7366.667	0.050	0.292	0.022	1.810
JJA	39.776	44.738	42.304	1.174	204.667	7366.667	0.050	**0.035**	0.039	2.373
SON	26.649	34.896	31.893	1.564	112.667	7366.667	0.050	0.359	0.023	1.310
Najaf: Min. Temperature										
DJF	1.407	9.306	4.778	1.798	84.667	7366.667	0.050	0.400	0.027	0.977
MAM	12.562	18.235	15.403	1.290	142.667	7366.667	0.050	0.162	0.032	1.650
JJA	23.716	29.053	26.460	1.214	304.667	7366.667	0.050	**0.004**	0.055	3.540
SON	14.954	20.925	18.073	1.408	187.333	7366.667	0.050	0.168	0.043	2.173

The (M-K) test shows non-significant increases in the yearly trends of maximum temperature and precipitation values. This is supported by the positive Z values recorded at all stations, with P-values > 0.05. The yearly precipitation trend in the Diwaniyah and Samawa governorates did not show a substantial reduction, as indicated by the negative Z values of -0.287 and -0.237; the results were corroborated by calculations using the Sine slope; this indicates that the trends did not exhibit a noteworthy rise or decline, leading to a conclusion of "no significant trend." This can be ascribed to the constantly stable meteorological conditions in the area. In contrast to the minimum temperatures, which experienced a substantial and conspicuous increase, the mean P-value for the trend in minimum temperature for certain regions over the summer season (June, July, and August) was determined to be below 0.05, showing a statistically significant rising trend at the 5% significance threshold; refer to Figure 7 and Table 7.

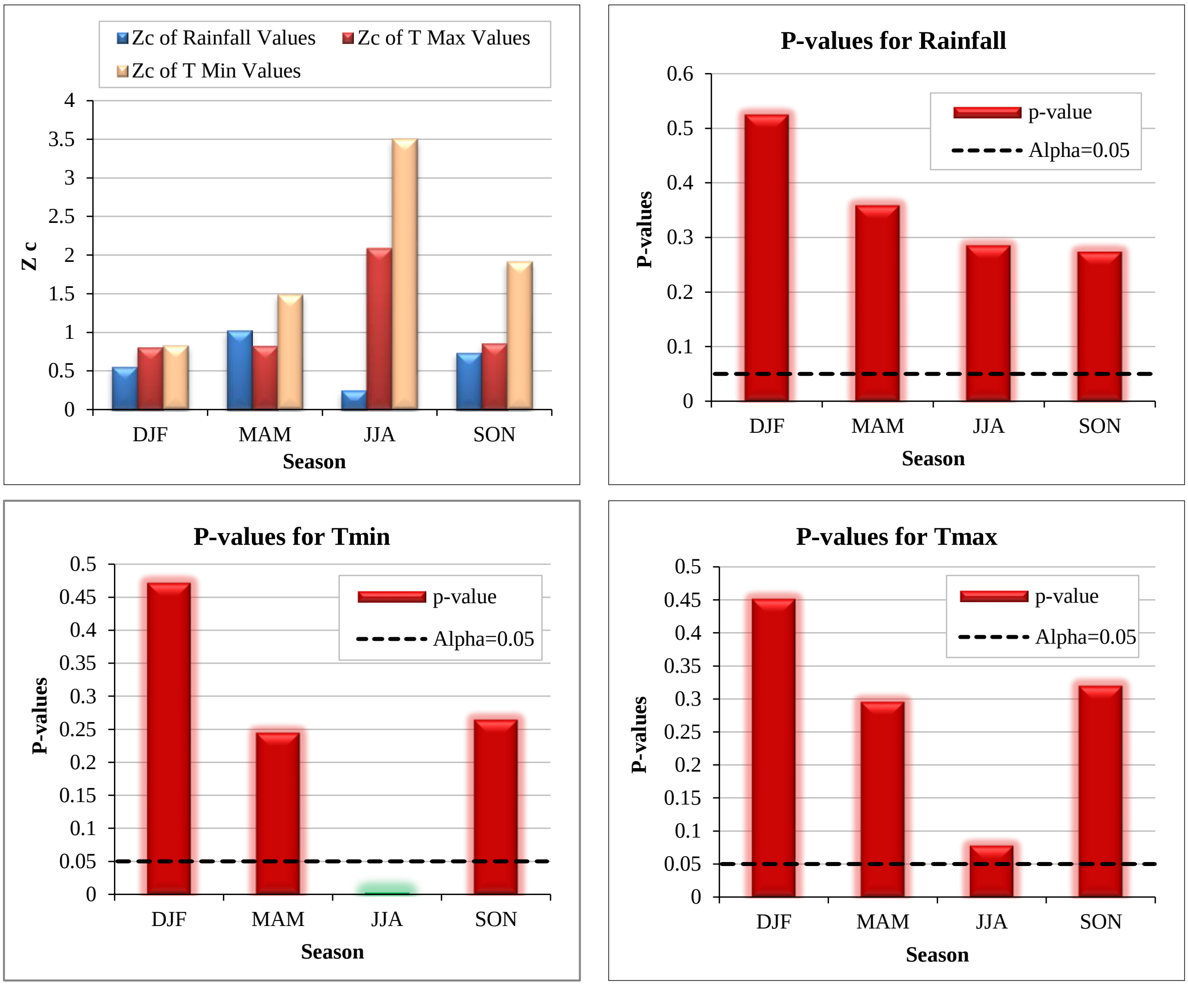

Figure 7. Average values of P and ZC for all climate stations for rainfall and minimum and maximum temperatures

3.3. Projection of Future Temperatures

3.3.1. Maximum Temperature (T max.)

Figure 8 and Table 8 illustrate the average monthly and seasonal variations in the Tmax measured for the future (2021-2060) under the SSP-245 and SSP-585 scenarios. The average monthly Tmax shows an increasing trend for SSP-245 and SSP-585 scenarios from 2021 to 2060. Seasonally, Tmax exhibits an upward trend, varying between +1.156 °C and +2.095 °C in the 2030s (2021–2040) and 2050s (2041–2060), respectively, under the SSP-245 scenario. In the SSP-585 scenario, the Tmax exhibits an upward trend, varying from +1.549 °C to +2.892 °C for the 2030s (2021–2040) and 2050s (2041–2060), respectively, relative to the baseline period.

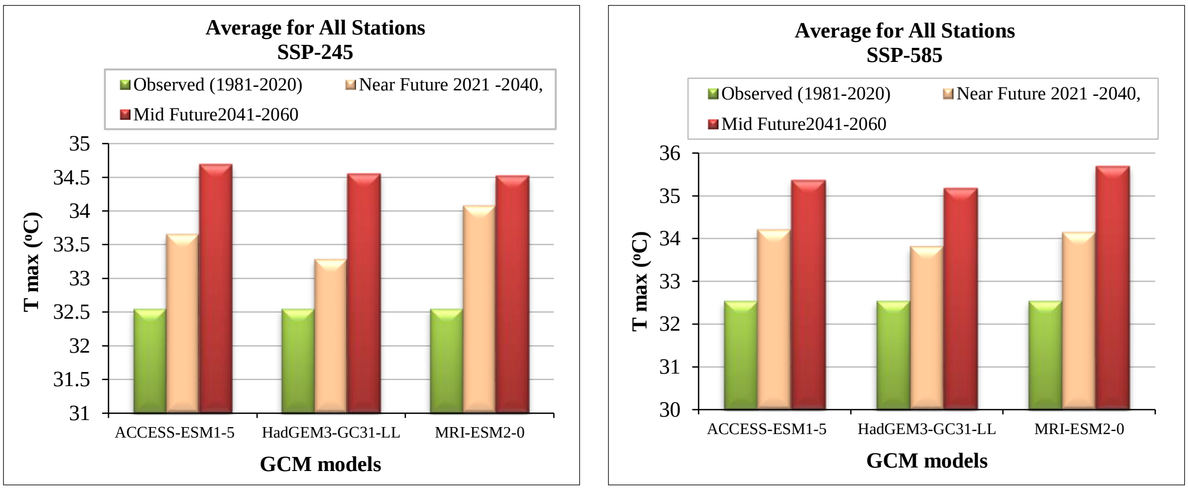

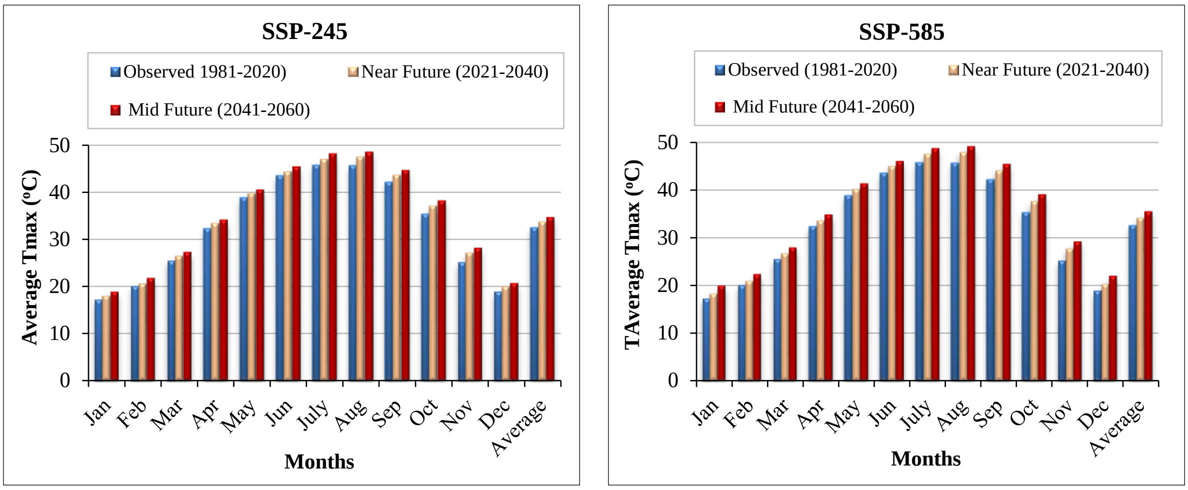

Figure 8. Comparison of the monthly average maximum temperature for three models and three periods, including the baseline period

Table 8. Alterations in climate variables within the related scenarios examined in the study

	ACCESS - ESM1-5				HadGEM3 - GC31-LL				MRI – ESM2-0				Average
	DJF	MAM	JJA	SON	DJF	MAM	JJA	SON	DJF	MAM	JJA	SON	
<u>Rainfall (SSP-245)</u>													
2021-2040	5.085	2.327	0.050	-0.401	12.553	3.266	0.044	3.428	-0.465	0.846	0.027	0.039	**2.233**
2041-2060	3.637	3.228	0.046	-1.189	6.355	1.173	0.048	4.843	3.700	0.550	0.022	1.440	**1.988**
<u>Rainfall (SSP-585)</u>													
2021-2040	4.765	0.523	0.029	0.141	14.178	3.605	0.019	4.812	4.367	1.891	0.027	-0.383	**2.831**
2041-2060	4.423	3.067	0.075	0.197	14.246	4.460	0.027	3.956	1.749	-0.218	0.046	-1.510	**2.543**
<u>Min. temp. (°C) (SSP-245)</u>													
2021-2040	1.3093	1.242	1.425	2.231	1.379	1.405	1.177	1.675	1.288	1.053	1.579	2.066	**1.486**
2041-2060	1.498	1.822	2.535	3.2369	2.581	2.247	2.193	2.757	1.676	1.071	2.338	2.917	**2.239**
<u>Min. temp. (°C) (SSP-585)</u>													
2021-2040	1.0349	1.319	1.833	2.3241	2.401	1.863	1.662	2.238	1.459	0.709	1.759	2.642	**1.770**
2041-2060	2.3967	2.426	3.386	4.0824	3.799	2.927	2.862	3.802	2.853	2.047	2.894	3.754	**3.102**
<u>Max. temp. (°C) (SSP-245)</u>													
2021-2040	0.946	0.813	0.811	2.010	-0.009	0.877	1.200	0.992	1.411	1.122	1.589	2.111	**1.156**
2041-2060	1.598	1.648	2.426	3.082	1.732	2.224	2.104	2.212	1.586	1.210	2.391	2.934	**2.095**
<u>Max. temp. (°C) (SSP-585)</u>													
2021-2040	1.089	1.638	1.835	2.241	0.638	1.376	1.701	1.545	1.344	0.586	1.760	2.832	**1.549**
2041-2060	2.541	2.361	2.769	3.732	2.021	2.653	2.883	3.083	3.299	2.202	3.068	4.092	**2.892**

It was also noted that the average monthly maximum (Tmax) for three models (ACCESS-ESM1-5, HadGEM3-GC13-LL, and MIR-ESM2-0) are (33.66, 33.29, and 34.08) °C, respectively, for the period (2021-2040), and for the period (2041-2060) are (34, 69, 34.55, and 34.52) °C, respectively, under SSP-245. Regarding SSP-585, they are (34.20, 33.81, and 34.14) °C, respectively, for the period (2021-2040), and (35.37, 35.18, and 35.69) °C, respectively, for the period (2041-2060). Compared to the baseline data, the average monthly Tmax was 32.55°C, rising to 33.71°C within the period (2021-2040) and continuing to rise to 34.64°C within the period (2041-2060) under SSP-245. For SSP-585, they are (32.55, 34.10, and 35.44) °C, respectively. The increase was insignificant for both scenarios, according to IPCC-TGICA (2007), which anticipated that the worldwide average surface air temperature would rise from +1.40°C to +5.80°C in the 2100s. This study is in agreement with the previous study by Mohammed and Hassan (2022) [27] at three meteorological stations located in southern Iraq., which showed that (T max) will increase from 1.41 °C to 1.50 °C in the RCP-4.5 and 5.67 °C to 5.91 °C in the RCP-8.5 emission scenarios.

Figure 9 shows the variations in Tmax for the two chosen periods compared to the baseline period. The graphic indicates distinct forecasting patterns for the three GCM models over various periods. These disparities suggest that it is challenging and unpredictable to forecast future temperature using individual GCM models, as each model may yield distinct predictions. MRI-ESM2-0 predicted the highest Tmax (+3.75 ºC) increase under SSP-585, recorded in autumn (SON) from 2041–2060. The highest decrease in Tmax (+0.59 ºC) was recorded using MRI-ESM2-0 in spring (MAM) for 2021-2040 under SSP-585.

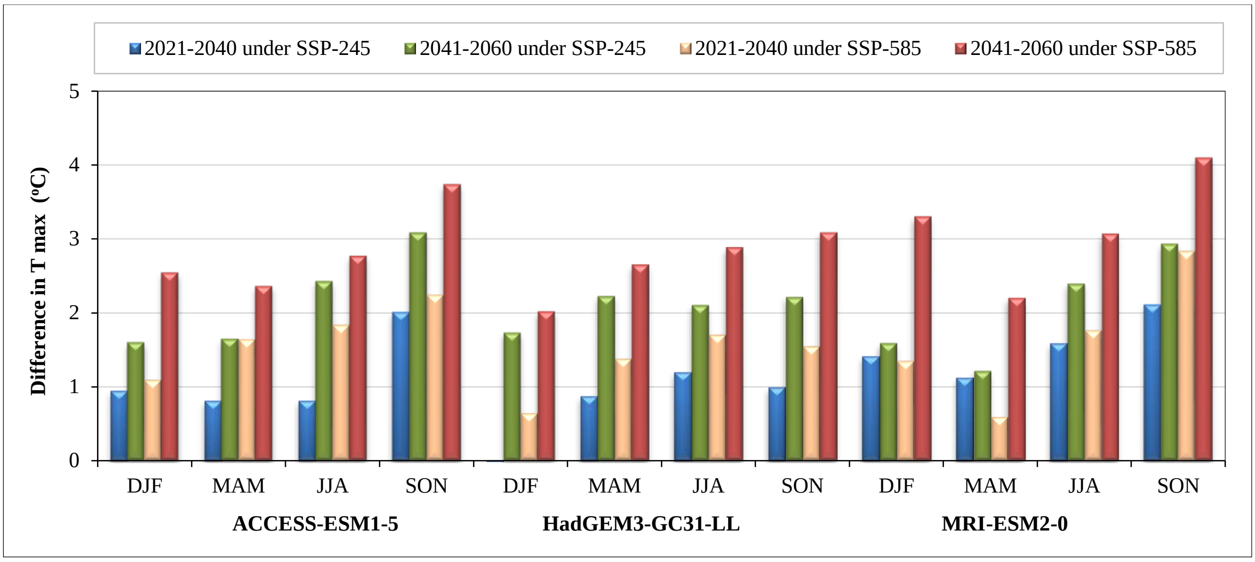

Figure 9. The disparities in seasonal (T max) between the projected timeframes (2021–2040 and 2041–2060) and the recorded period (1981–2020)

3.3.2. Minimum Temperature (T min.)

The Tmin exhibits an upward tendency in overall annual future periods for SSP-245 and SSP-585 scenarios. Figure 10 and Table 8 show the highest increment of average Tmin was projected on the PSS-585 scenario in the period (2041-2060), about +3.102 °C, and +1.770 °C in the period (2021-2040) in the same scenario. For scenario SSP-245, the results showed an average Tmin increase of +1.486 °C to +2.239 °C from the 2030s to the 2050s, respectively.

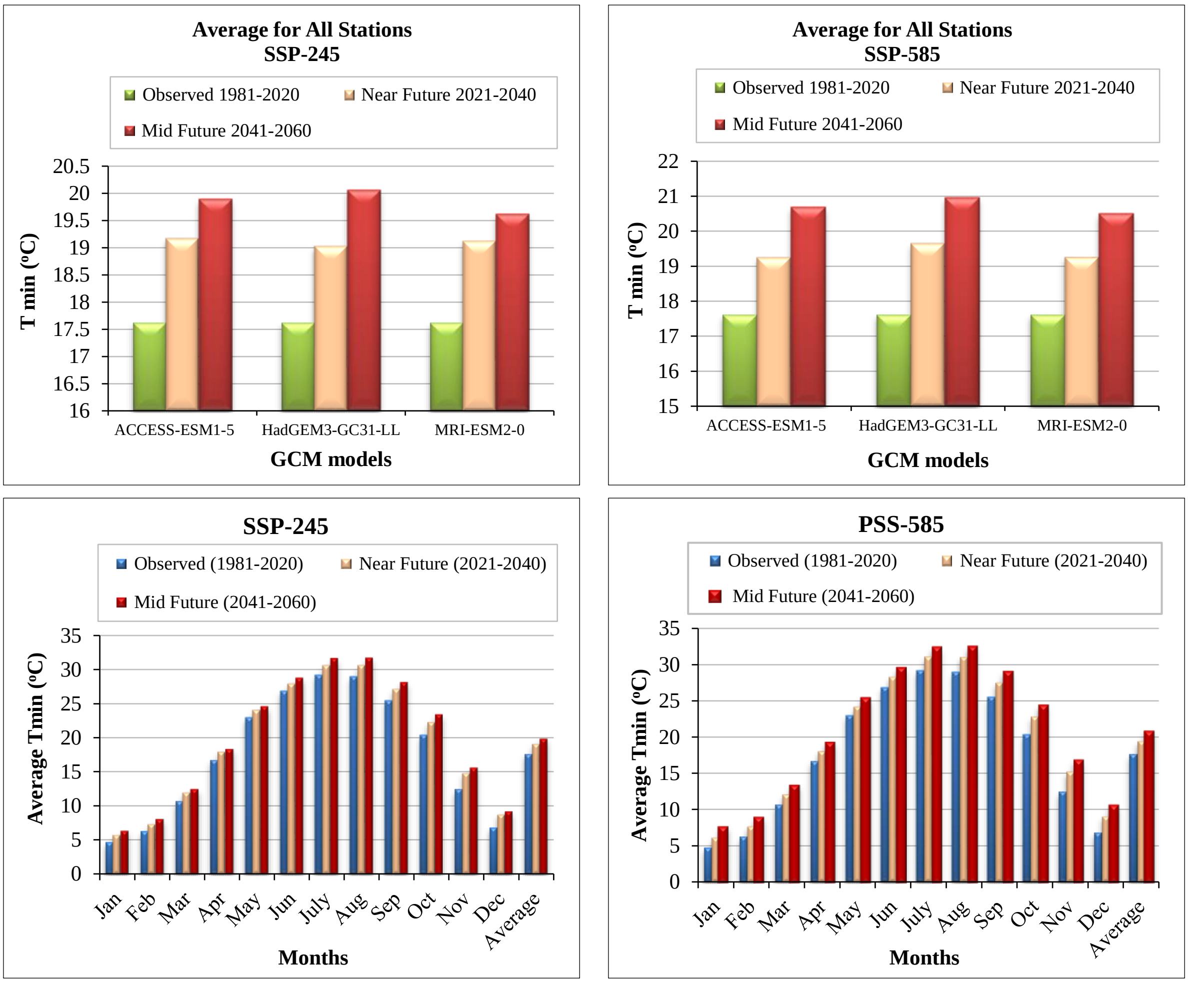

Figure 10. Comparison of the monthly average minimum temperature for three models and three periods, including the baseline period

It was also noted that the average monthly Tmin for the three models (ACCESS-ESM1-5, HadGEM3-GC13-LL, and MIR-ESM2-0) are (19.17, 19.03, and 19.12) °C, respectively, for the period (2021-2040), and for the period (2041-2060) are (19.89, 20.06, and 19.62) °C, respectively, under SSP-245. Regarding SSP-585, they are (19.25, 19.66, and 19.26) °C, respectively, for the period (2021-2040), and (20.69, 20.97, and 20.51) °C, respectively, for the period (2041-2060).

Compared to the baseline data, the average monthly Tmin was 17.62 °C, rising to 19.11 °C within the period (2021-2040) and continuing to rise to 19.86 °C within the period (2041-2060) under SSP-245. For SSP-585, they are (17.62, 19.39, and 20.72) °C, respectively.

The study is consistent with the research conducted by Z. M. Mohammed and Hassan (2022) [27] in the same basin. Their analysis indicates that the projected mean annual Tmax is displaying a rising pattern. The study is consistent with the outcome by Mukheef et al. (2024) [20], done in Iraq's western and central regions, which indicates that the predicted mean annual Tmax is increasing. The Tmin showed a steadily increasing trend, which aligns with previous studies in various parts of Iraq. The results indicate that the average annual Tmax and Tmin will increase at all selected locations across the three future eras by a range of 0.94 to 4.98 °C by the end of the twenty-first century [28].

Figure 11 illustrates the variations in Tmin between the baseline period (1981-2020) and the subsequent periods (2021-2040) and (2041-2060). The values of three models significantly increased, especially during 2021-2060 under the influence scenario (SSP-585). The MRI-ESM2-0 model predicted the lowest Tmin (+0.71 °C) increase under SSP-585, recorded in spring (MAM) from 2021 to 2040. The highest increase in Tmin (+4.08 °C) was recorded using ACCESS-ESM1-5 in autumn (SON) for 2021-2040 under scenario SSP-585.

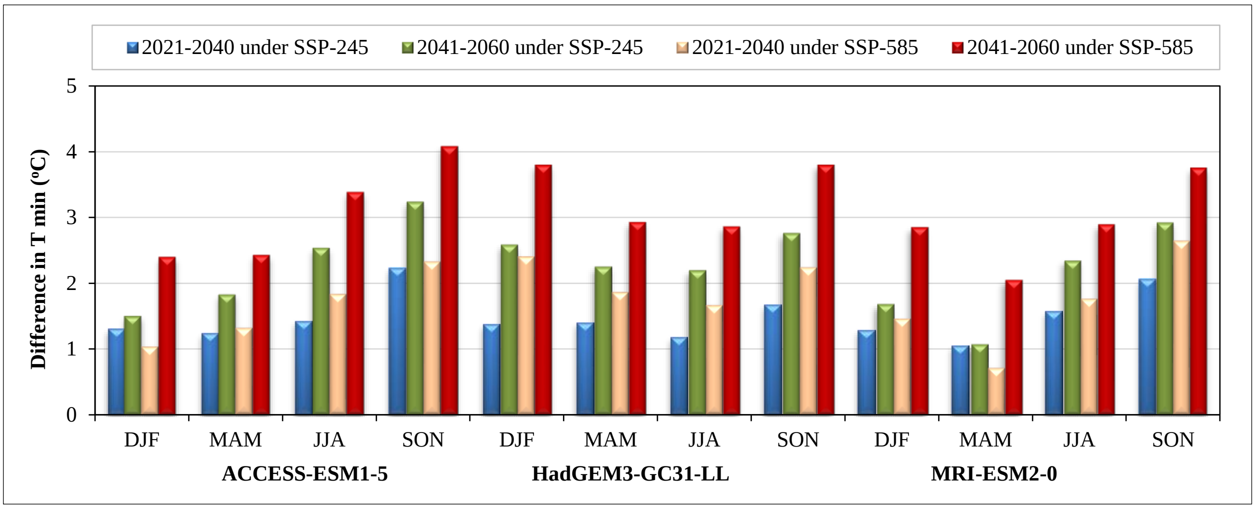

Figure 11. The disparities in seasonal (Tmin) between the projected timeframes (2021–2040 and 2041–2060) and the recorded period (1981–2020)

4. Projection of Future Precipitation

Figure 12 and Table 8 Their results indicate rainfall fluctuations for 2021-2060, with an upward trend under SSP-245 and SSP-585 scenarios. In the SSP-245 scenario, the annual rainfall increase varies from +2.233 mm (2021-2040) to +1.988 mm (2041-2060). The augmentation in the SSP-585 scenario varies from +2.831 mm (2021-2040) to +2.543 mm (2041-2060).

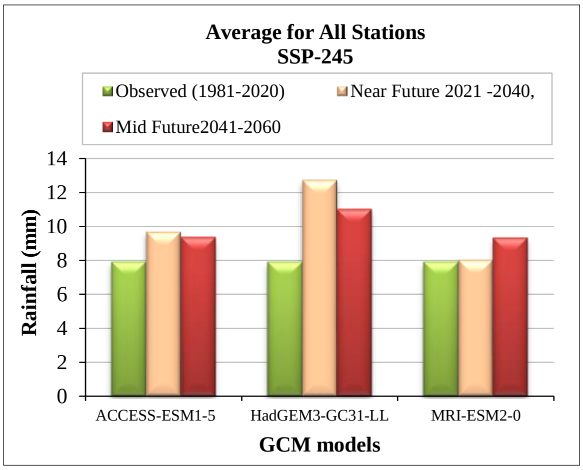

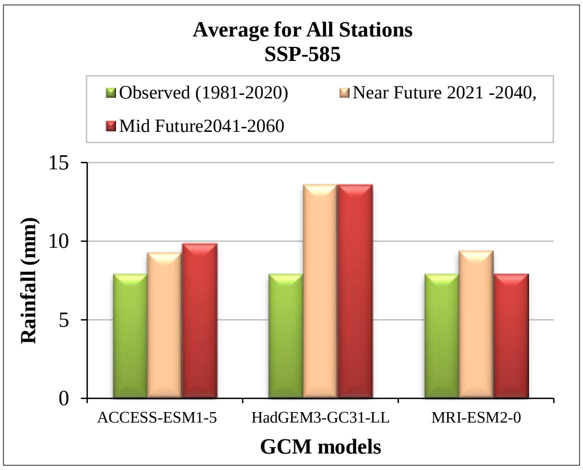

Figure 12. Comparison of the monthly average rainfall for three models and three periods, including the baseline period

It was also noted that the monthly rainfall averages for the three models (ACCESS-ESM1-5, HadGEM3-GC13-LL, and MIR-ESM2-0) are 9.67, 12.73, and 8.02 mm, respectively, for the period (2021-2040), and for the period (2041-2060) are (9.34, 11.01, and 9.33) mm, respectively, under SSP-245. Regarding SSP-585, they are (9.27, 13.56, and 9.38) mm, respectively, for the period (2021-2040), and (9.85, 13.58, and 7.92) mm, respectively, for the period (2041-2060). Compared to the baseline data, the average monthly rainfall increased from 7.91 mm to 10.11 mm during 2021-2040, then decreased to 9.89 mm in 2041-2060 under SSP-245. The temperatures for SSP-585 are 7.91 °C, 10.74 °C, and 10.45 °C, respectively.

The outcomes of this study were consistent with the prior studies conducted in close proximity to the study site. Predictions using RCP4.5 indicate that rainy years are expected to occur between 2029 and 2034, as well as between 2050 and 2054. These predictions include both the yearly and winter month averages of precipitation. According to the RCP-8.5 scenario, there would be periods of rainfall from 2025 to 2034 and 2050 to 2055, followed by periods of drought [20, 28, 51]. The variability in precipitation stemming from climate change leads to water scarcity, hence significantly impacting ecosystems characterized by rainfall and water resources [52]. Additionally, climate change is anticipated to impact stream flow and surface water distribution significantly [53].

Figure 13 illustrates the fluctuation of rainfall at each of the seven climatic stations, the impact of global warming on rainfall volume, and the comparison between the baseline data and future projected data under the SSP-245 and SSP-585 scenarios. Figure 14 shows the monthly rainfall average for all stations within the study area during three important periods.

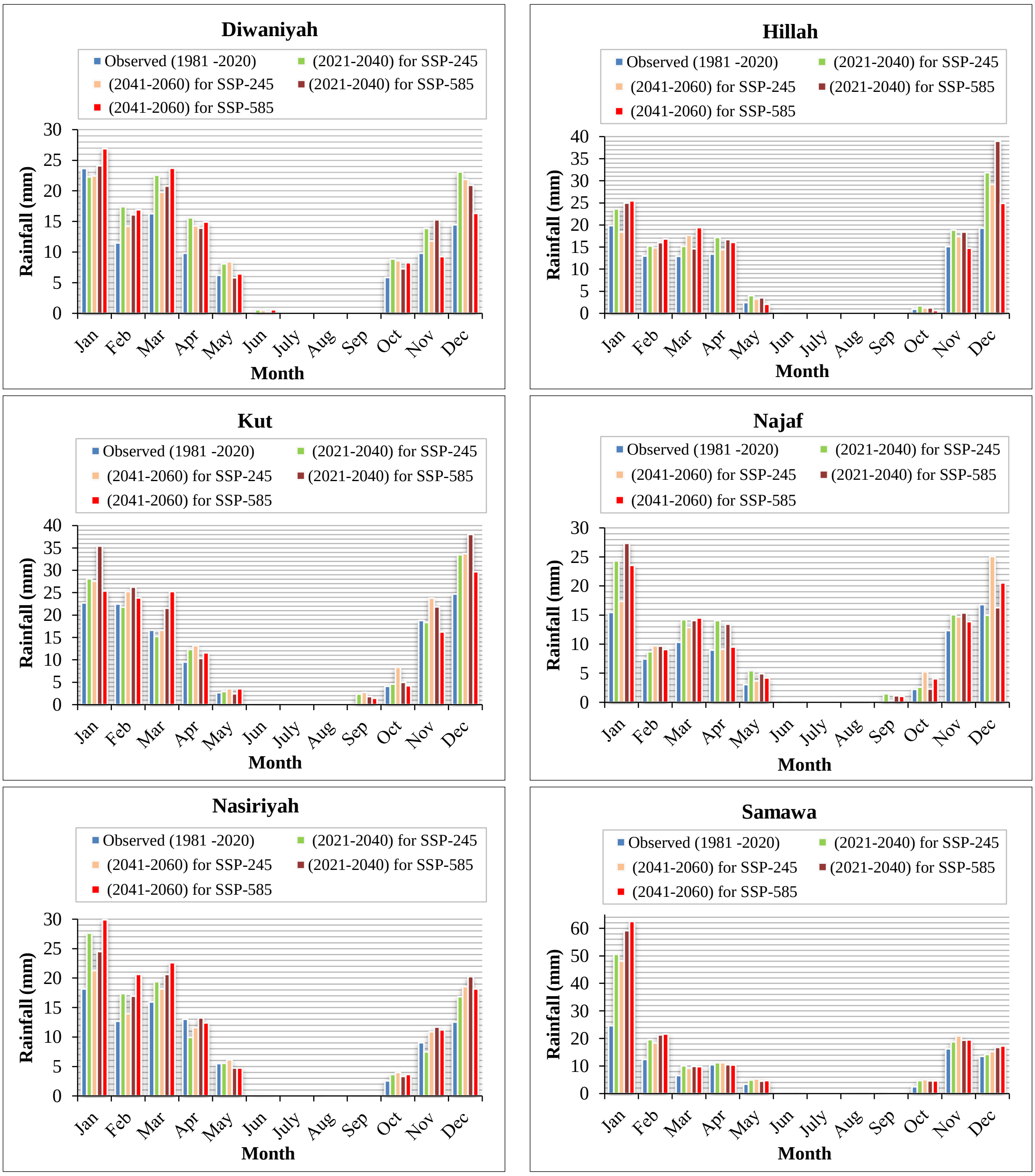

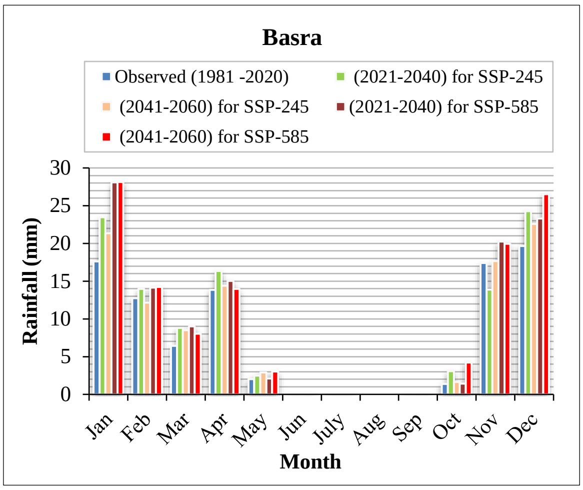

Figure 13. illustrates the rainfall variability at each of the seven locations, highlighting the impact of global warming on rainfall quantities

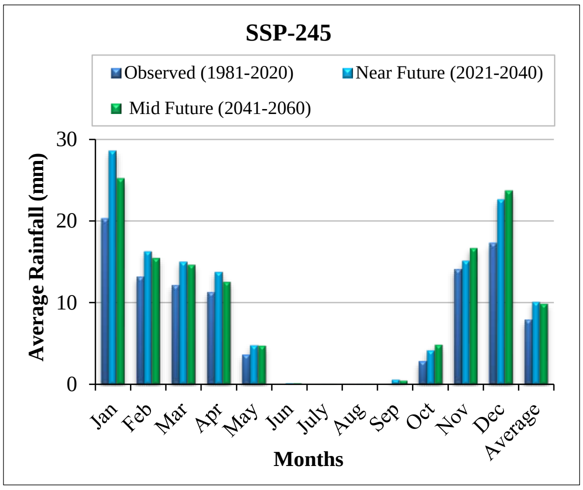

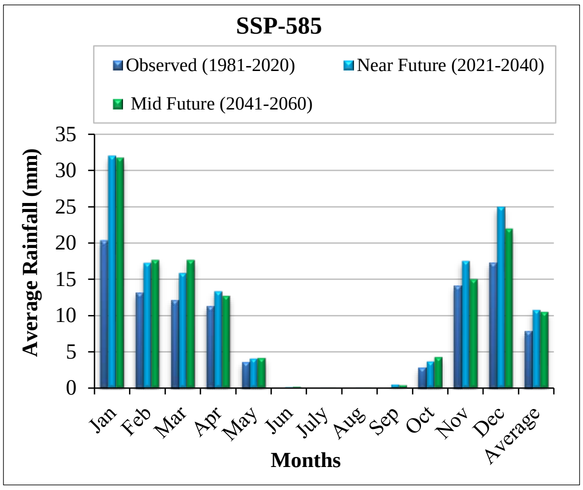

Figure 14. Monthly rainfall average for all stations within the study area during three important periods

Figure 15 displays the variations in seasonal precipitation for two chosen periods compared to the baseline period. The graphic indicates distinct forecasting patterns for the three GCM models over various periods. These discrepancies indicate that forecasting future rainfall using individual GCM models is difficult and uncertain, as each model may produce divergent projections. HadGEM3-GC31-LL, a climate model, predicted the largest rise in rainfall of 14.25 mm under the SSP-585 scenario. This increase occurred in the winter season (DJF) between 2041 and 2060. The greatest reduction in rainfall (1.51 mm) was observed during the autumn season (SON) from 2041 to 2060 using the MRI-ESM2-0 model.

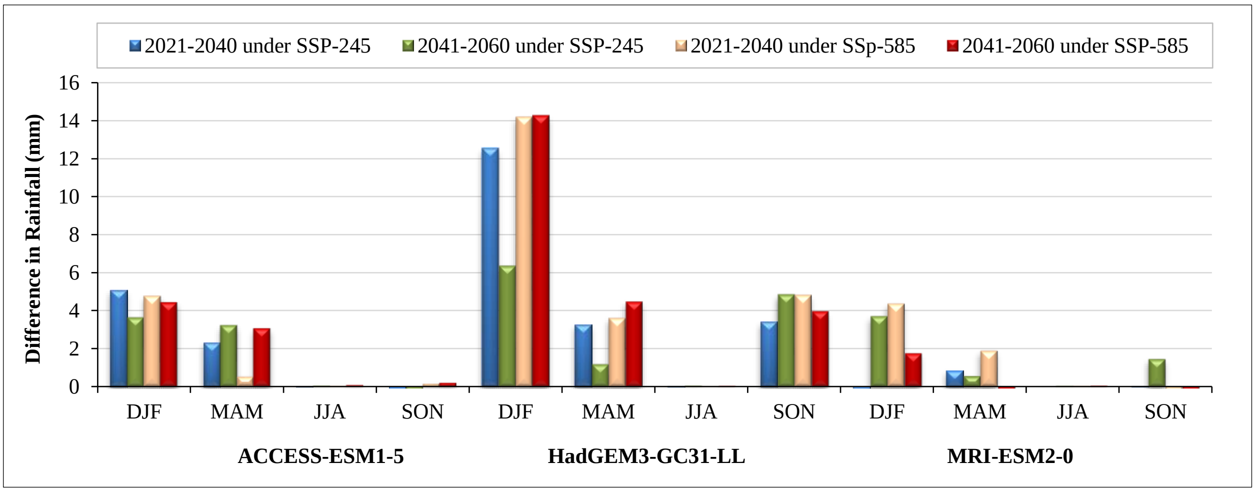

Figure 15. The disparities in seasonal precipitation between the projected timeframes (2021–2040 and 2041–2060) and the recorded period (1981–2020)

Figure 16 illustrates the variation in rainfall rates from 1981 to 2060, impacted by the SSP-245 and SSP-585 scenarios. It is noted from the trend line of the linear prediction that rainfall increases gradually during the base period and then reaches its highest amount in 2020 and then decreases until 2060. This will cause a future decrease in water imports in the region and requires decision-makers to take the necessary measures and use the water harvesting process to benefit from it during water demand.

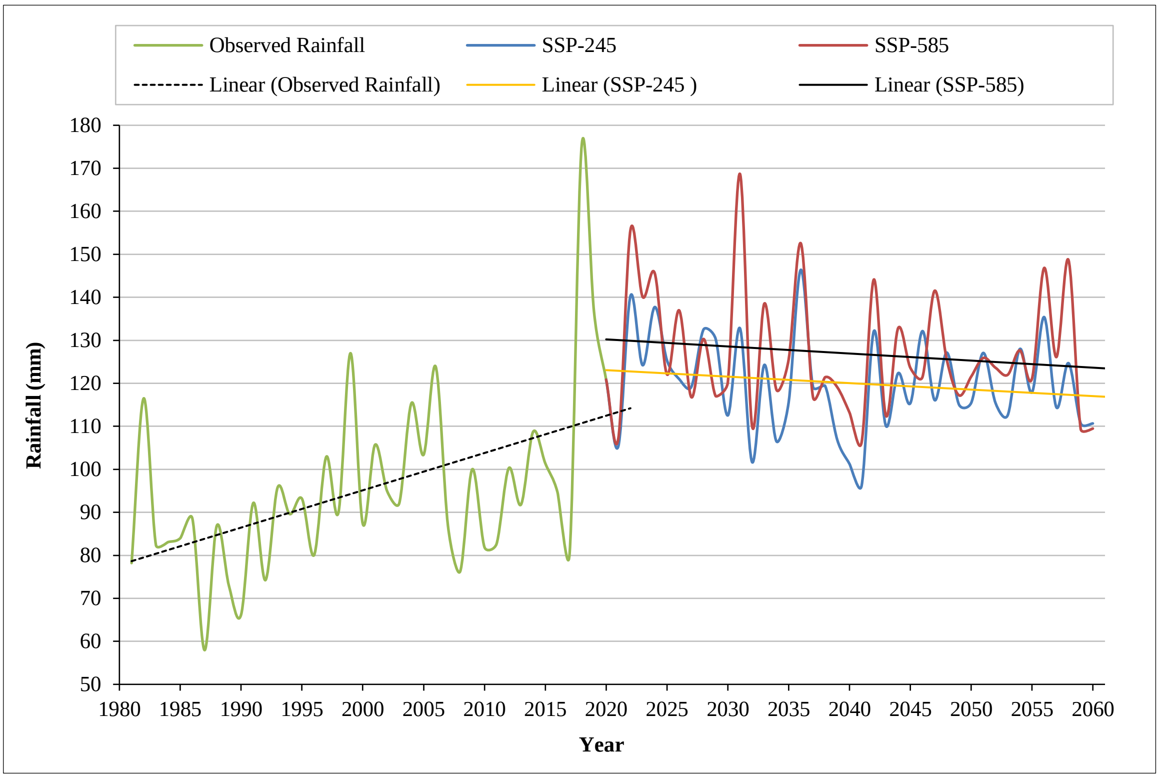

Figure 16. Future projection of average precipitation

5. Conclusions

The analysis of climate variables revealed a slight increase in precipitation and a general rise in average annual Tmax and Tmin in the study area from 1981 to 2020. The results of this analysis indicate a non-significant increase in precipitation and a considerable increase in both Tmax and Tmin during the 2030s and 2050s.

The average monthly increase in Tmax varies from +1.156 °C (2021–2040) to +2.095 °C (2041–2060) under the SSP-245 scenario, compared to the baseline period. The temperature increase for the SSP-585 scenario varies from +1.549 °C (2021–2040) to +2.892 °C (2041–2060). The largest increase in the maximum temperature occurred during September, October, and November (the autumn season, also known as SON), reaching a value of +3.732 °C in the SSP-585 scenario.

Tmin exhibits an upward tendency in overall annual future periods for SSP-245 and SSP-585 scenarios. The most significant increase in average Tmin was projected under the SSP-585 scenario from 2041 to 2060, about +3.102 °C and +1.770 °C (2021-2040) in the same scenario. For scenario SSP-245, the results showed an increase in the average Tmin of +1.486 °C to +2.239 °C from the 2030s to the 2050s, respectively.

Projected increases in precipitation during the winter season (DJF) are expected to range from +4 to +14 mm. The extensive analysis (2021–2060) of seasonal percentage changes in precipitation reveals an upward trend for SSP-245 and SSP-585 scenarios. Under the SSP-245 scenario, the annual increase in precipitation varies from +2.233 mm (2021–2040) to +1.988 mm (2041-2060). The increment for the SSP-585 scenario varies from +2.831 mm (2021-2040) to +2.543 mm (2041-2060). This increase is considered insignificant, an indicator that raises concerns about the drought occurrence. The region's complex pattern of low rainfall could directly impact agricultural production, food availability, and local ecosystems. The study's strength lies in its holistic approach, which reduces model uncertainty by utilizing several GCM ensembles. Integrating hydrological models with GCM models will enhance this study. Additional investigation will be necessary to consider the constraints of this study in answering all ambiguities. Moreover, future studies should examine the effects of other climate change adaptation strategies. This study's findings can be used to develop strategies for alleviating climate change.

6. Declarations

6.1. Author Contributions

Conceptualization, S.H.H. and H.H.A.; methodology, S.H.H.; software, S.H.H.; validation, S.H.H., H.H.A., and F.M.A.; formal analysis, S.H.H., H.H.A., and F.M.A.; investigation, S.H.H.; resources, S.H.H.; data curation, S.H.H.; writing—original draft preparation, S.H.H.; writing—review and editing, S.H.H., H.H.A., and F.M.A.; visualization, S.H.H.; supervision, H.H.A. and F.M.A.; project administration, S.H.H.; funding acquisition, S.H.H. and H.H.A. All authors have read and agreed to the published version of the manuscript.

6.2. Data Availability Statement

The data presented in this study are available in the article.

6.3. Funding

The authors received no financial support for the research, authorship, and/or publication of this article.

6.4. Conflicts of Interest

The authors declare no conflict of interest.

7. References

[1] Oo, H. T., Zin, W. W., & Kyi, C. C. T. (2019). Assessment of Future Climate Change Projections Using Multiple Global Climate Models. Civil Engineering Journal (Iran), 5(10), 2152–2166. doi:10.28991/cej-2019-03091401.

[2] Kundu, A., Dwivedi, S., & Chandra, V. (2014). Precipitation Trend Analysis over Eastern Region of India Using Cmip5 Based Climatic Models. The International Archives of the Photogrammetry, Remote Sensing and Spatial Information Sciences, XL–8, 1437–1442. doi:10.5194/isprsarchives-xl-8-1437-2014.

[3] USAID. (2017). Climate Risk Profile: Iraq. United States Agency for International Development (USAID), Washington, United States. Available online: https://www.climatelinks.org/resources/climate-change-risk-profile-iraq (accessed on November 2024).

[4] Cooke, K. (2018). Iraq's climate stresses are set to worsen. PreventionWeb, Geneva, Switzerland. Available online: https://www.preventionweb.net/news/iraqs-climate-stresses-are-set-worsen (accessed on November 2024).

[5] Agence France Presse. (2018). Iraq's cultivated areas reduced by half as drought tightens grip. Agence France Presse, Paris, France. Available online: https://www.thenationalnews.com/world/mena/iraq-s-cultivated-areas-reduced-by-half-as-drought-tightens-grip-1.756996 (accessed on November 2024).

[6] United Nations Iraq. (2020). Iraq mulls tackling its methane problem and reaping major benefits along the way. United Nations Iraq, Baghdad, Iraq. Available online: https://www.uniraq.org/index.php?option=com_k2&view=item&id=12935:iraq-mulls-tackling-its-methane-problem-and-reaping-major-benefits-along-the-way&Itemid=605&lang=en (accessed on November 2024).

[7] Ritchie, H., Roser, M., & Rosado, P. (2020). CO_2 and greenhouse gas emissions. Our world in data, Oxford, United Kingdom.

[8] Masson-Delmotte, V. P., Zhai, P., Pirani, S. L., Connors, C., Péan, S., Berger, N., ... & Scheel Monteiro, P. M. (2021). IPCC, 2021: Summary for policymakers. in: Climate change 2021: The physical science basis. contribution of working group i to the sixth assessment report of the intergovernmental panel on climate change. Cambridge University Press, Cambridge, United Kingdom and New York, United States.

[9] Lee, H., Calvin, K., Dasgupta, D., Krinner, G., Mukherji, A., Thorne, P., ... & Zommers, Z. (2023). Climate change 2023: synthesis report. Contribution of working groups I, II and III to the sixth assessment report of the intergovernmental panel on climate change. The Australian National University, Canberra, Australia.

[10] Waha, K., Krummenauer, L., Adams, S., Aich, V., Baarsch, F., Coumou, D., Fader, M., Hoff, H., Jobbins, G., Marcus, R., Mengel, M., Otto, I. M., Perrette, M., Rocha, M., Robinson, A., & Schleussner, C. F. (2017). Climate change impacts in the Middle East and Northern Africa (MENA) region and their implications for vulnerable population groups. Regional Environmental Change, 17(6), 1623–1638. doi:10.1007/s10113-017-1144-2.

[11] Calvin, K., Dasgupta, D., Krinner, G., Mukherji, A., Thorne, P. W., Trisos, C., Romero, J., Aldunce, P., Barrett, K., Blanco, G., Cheung, W. W. L., Connors, S., Denton, F., Diongue-Niang, A., … Ha, M. (2023). IPCC, 2023: Climate Change 2023: Synthesis Report. Contribution of Working Groups I, II and III to the Sixth Assessment Report of the Intergovernmental Panel on Climate Change. Intergovernmental Panel on Climate Change (IPCC), Geneva, Switzerland. doi:10.59327/ipcc/ar6-9789291691647.

[12] Stepanyan, V., Abdih, Y., Al-Hassan, A., Gerling, K., Saksonovs, S., Baum, A., Anderson, G., Agoumi, L., Andaloussi, M., Chen, C., Sakha, S., Saliba, F., Sanchez, J., & Duenwald, C. (2022). Feeling the Heat: Adapting to Climate Change in the Middle East and Central Asia. Departmental Papers, 2022(008), 1. doi:10.5089/9781513591094.087.

[13] IPCC. (2021). Summary for Policymakers. Climate Change 2021: The Physical Science Basis. Contribution of Working Group I to the Sixth Assessment Report of the Intergovernmental Panel on Climate Change. Cambridge University Press, Cambridge, United Kingdom and New York, United States. doi:10.1017/9781009157896.001.

[14] Phuong, D. N. D., Duong, T. Q., Liem, N. D., Tram, V. N. Q., Cuong, D. K., & Loi, N. K. (2020). Projections of future climate change in the VU Gia Thu Bon river basin, Vietnam by using statistical downscaling model (SDSM). Water (Switzerland), 12(3), 755. doi:10.3390/w12030755.

[15] Semenov, M. A., & Barrow, E. M. (2002). A stochastic weather generator for use in climate impact studies. User Man Herts United Kingdom.

[16] Wilby, R. L., Dawson, C. W., & Barrow, E. M. (2007). Statistical downscaling model (SDSM), version 4.2. Department of Geography, Lancaster University, Lancashire, United Kingdom.

[17] Gao, C., He, Z., Pan, S., Xuan, W., & Xu, Y. P. (2020). Effects of climate change on peak runoff and flood levels in Qu River Basin, East China. Journal of Hydro-Environment Research, 28, 34–47. doi:10.1016/j.jher.2018.02.005.

[18] Navid, S., Jahansouz, M., Soufizadeh, S., & Ghafari, M. (2024). Predicting the Changes of Climatic Parameters in Alborz Province by Using the LARS-WG Model with Risk Management Approach. The Quarterly Journal of Insurance & Agriculture (QJIA), 13(1), 1-18.

[19] Jimenez Osorio, D. A., Menapace, A., Zanfei, A., de Andrade Pinto, E. J., & Brentan, B. (2023). Statistical and Machine Learning Downscaling Methods to Assess Changes to Rainfall Amounts and Frequency in Climate Change Context - CMIP 6. doi:10.5194/hess-2023-55.

[20] Mukheef, R. A. H., Hassan, W. H., & Alquzweeni, S. (2024). Projections of temperature and precipitation trends using CMhyd under CMIP6 scenarios: A case study of Iraq's Middle and West. Atmospheric Research, 306, 107470. doi:10.1016/j.atmosres.2024.107470.

[21] Kh. Muhaisen, N., Sh. Khayyun, T., Mukhtar, M. Al, & Hassan, W. H. (2024). Forecasting changes in precipitation and temperatures of a regional watershed in Northern Iraq using LARS-WG model. Open Engineering, 14(1), 20220567. doi:10.1515/eng-2022-0567.

[22] Mohammed, R., & Scholz, M. (2024). Climate Change Scenarios for Impact Assessment: Lower Zab River Basin (Iraq and Iran). Atmosphere, 15(6), 673. doi:10.3390/atmos15060673.

[23] Osman, Y., Abdellatif, M., Al-Ansari, N., Knutsson, S., & Jawad, S. (2017). Climate change and future precipitation in an arid environment of the MIDDLE EAST: CASE study of Iraq. Journal of Environmental Hydrology, 25(3), 1-21.

[24] Kriegler, E., O'Neill, B. C., Hallegatte, S., Kram, T., Lempert, R. J., Moss, R. H., & Wilbanks, T. (2012). The need for and use of socio-economic scenarios for climate change analysis: A new approach based on shared socio-economic pathways. Global Environmental Change, 22(4), 807–822. doi:10.1016/j.gloenvcha.2012.05.005.

[25] O'Neill, B. C., Kriegler, E., Riahi, K., Ebi, K. L., Hallegatte, S., Carter, T. R., Mathur, R., & van Vuuren, D. P. (2013). A new scenario framework for climate change research: the concept of shared socioeconomic pathways. Climatic Change, 122(3), 387–400. doi:10.1007/s10584-013-0905-2.

[26] Van Vuuren, D. P., Riahi, K., Moss, R., Edmonds, J., Thomson, A., Nakicenovic, N., Kram, T., Berkhout, F., Swart, R., Janetos, A., Rose, S. K., & Arnell, N. (2012). A proposal for a new scenario framework to support research and assessment in different climate research communities. Global Environmental Change, 22(1), 21–35. doi:10.1016/j.gloenvcha.2011.08.002.

[27] Mohammed, Z. M., & Hassan, W. H. (2022). Climate change and the projection of future temperature and precipitation in southern Iraq using a LARS-WG model. Modeling Earth Systems and Environment, 8(3), 4205–4218. doi:10.1007/s40808-022-01358-x.

[28] Hassan, W. H., Nile, B. K., Kadhim, Z. K., Mahdi, K., Riksen, M., & Thiab, R. F. (2023). Trends, forecasting and adaptation strategies of climate change in the middle and west regions of Iraq. SN Applied Sciences, 5(12), 312. doi:10.1007/s42452-023-05544-z.

[29] Lee, J. Y., Marotzke, J., Bala, G., Cao, L., Corti, S., Dunne, J. P., ... & Zhou, T. (2021). Future global climate: scenario-based projections and near-term information. In Climate change 2021: The physical science basis. Contribution of working group I to the sixth assessment report of the intergovernmental panel on climate change. Cambridge University Press, Cambridge, United Kingdom.

[30] FAO. (2024). Enhancing Climate-Resilient Agriculture in Southern Iraq. Food and Agriculture organization of the United Nations (FAO), Rome, Italy. Available online: https://openknowledge.fao.org/server/api/core/bitstreams/29700ecb-bfc4-4de9-bb2e-efbf88c1f178/content (accessed on November 2024).

[31] Saud, S., Wang, D., Fahad, S., Alharby, H. F., Bamagoos, A. A., Mjrashi, A., Alabdallah, N. M., AlZahrani, S. S., AbdElgawad, H., Adnan, M., Sayyed, R. Z., Ali, S., & Hassan, S. (2022). Comprehensive Impacts of Climate Change on Rice Production and Adaptive Strategies in China. Frontiers in Microbiology, 13, 926059. doi:10.3389/fmicb.2022.926059.

[32] Ali, S. H., Qubaa, A. R., & Al-Khayat, A. B. M. (2024). Climate Change and its Potential Impacts on Iraqi Environment: Overview. IOP Conference Series: Earth and Environmental Science, 1300(1), 12010. doi:10.1088/1755-1315/1300/1/012010.

[33] Berkofsky, L. (2019). Desert Meteorology. Settling the Desert, 97–116. Cambridge University Press, Cambridge, United Kingdom. doi:10.4324/9780429287886-8.

[34] Rahimi, M., Yazdani, M. R., Asadi, M., & Karem, A. (2014). Temporal and spatial variability of dust storm events in West Asia (Iran and Iraq border). International Journal of Civil and Environmental Research, 1(3), 100–109.

[35] Al-Ansari, N. (2020). Topography and Climate of Iraq. Journal of Earth Sciences and Geotechnical Engineering, 11(2), 1–13. doi:10.47260/jesge/1121.

[36] Al-Ansari, N., & Knutsson, S. (2011). Toward Prudent management of Water Resources in Iraq. Journal of Advanced Science and Engineering Research, 1(1), 53–67.

[37] Zandwijk, A., Monji, F., Mento, L., Opstal, R., Mahdi, I. K., & Snertlage, J. (2021). Water and Saline Agriculture in Central-Southern Iraq- A scoping study on the conditions, solutions, and actors in the field of saline farming. Dutch Embassy, Bagdad, Iraq.

[38] Peel, M. C., Finlayson, B. L., & McMahon, T. A. (2007). Updated world map of the Köppen-Geiger climate classification. Hydrology and Earth System Sciences, 11(5), 1633–1644. doi:10.5194/hess-11-1633-2007.

[39] Birpınar, M. E., Kızılöz, B., & Şişman, E. (2023). Classic trend analysis methods' paradoxical results and innovative trend analysis methodology with percentile ranges. Theoretical and Applied Climatology, 153(1–2), 1–18. doi:10.1007/s00704-023-04449-6.

[40] Esit, M. (2023). Investigation of innovative trend approaches (ITA with significance test and IPTA) comparing to the classical trend method of monthly and annual hydrometeorological variables: A case study of Ankara region, Turkey. Journal of Water and Climate Change, 14(1), 305–329. doi:10.2166/wcc.2022.356.

[41] Dong, Z., Jia, W., Sarukkalige, R., Fu, G., Meng, Q., & Wang, Q. (2020). Innovative trend analysis of air temperature and precipitation in the jinsha river basin, china. Water (Switzerland), 12(11), 3293. doi:10.3390/w12113293.

[42] Mann, H. B. (1945). Nonparametric Tests Against Trend. Econometrica, 13(3), 245. doi:10.2307/1907187.

[43] Kendall, M.G. (1975) Rank Correlation Methods (4th Ed.). Charles Griffin, London, United Kingdom.

[44] Sen, P. K. (1968). Estimates of the Regression Coefficient Based on Kendall's Tau. Journal of the American Statistical Association, 63(324), 1379–1389. doi:10.1080/01621459.1968.10480934.

[45] Praveen, B., Talukdar, S., Shahfahad, Mahato, S., Mondal, J., Sharma, P., Islam, A. R. M. T., & Rahman, A. (2020). Analyzing trend and forecasting of rainfall changes in India using non-parametrical and machine learning approaches. Scientific Reports, 10(1), 10342. doi:10.1038/s41598-020-67228-7.

[46] He, M., & Gautam, M. (2016). Variability and trends in precipitation, temperature and drought indices in the state of California. Hydrology, 3(2), 14. doi:10.3390/hydrology3020014.

[47] Semenov, M. A., & Stratonovitch, P. (2015). Adapting wheat ideotypes for climate change: Accounting for uncertainties in CMIP5 climate projections. Climate Research, 65, 123–139. doi:10.3354/cr01297.

[48] Ferreira, G. W. de S., Reboita, M. S., Ribeiro, J. G. M., & de Souza, C. A. (2023). Assessment of Precipitation and Hydrological Droughts in South America through Statistically Downscaled CMIP6 Projections. Climate, 11(8), 166. doi:10.3390/cli11080166.

[49] Moriasi, D. N., Arnold, J. G., Van Liew, M. W., Bingner, R. L., Harmel, R. D., & Veith, T. L. (2007). Model evaluation guidelines for systematic quantification of accuracy in watershed simulations. Transactions of the ASABE, 50(3), 885–900. doi:10.13031/2013.23153.

[50] Disasa, K. N., Yan, H., Wang, G., Zhang, J., Zhang, C., Zhu, X., Xue, R., Wang, B., & Bao, R. (2024). Trend Analysis and Projection of Climate Variables Using the LARS-WG Model in Coastal Areas of China, Researchsquare (Preprint), 1-38. doi:10.21203/rs.3.rs-4015632/v1.

[51] Hashim, B. M., Alnaemi, A. N. A., Hussain, B. A., Abduljabbar, S. A., Doost, Z. H., & Yaseen, Z. M. (2024). Statistical downscaling of future temperature and precipitation projections in Iraq under climate change scenarios. Physics and Chemistry of the Earth, 135, 103647. doi:10.1016/j.pce.2024.103647.

[52] Daba, M. H., Ayele, G. T., & You, S. (2020). Long-term homogeneity and trends of hydroclimatic variables in upper awash river basin, Ethiopia. Advances in Meteorology, 2020(1), 8861959. doi:10.1155/2020/8861959.

[53] Daba, M. H., & You, S. (2020). Assessment of climate change impacts on river flow regimes in the upstream of Awash basin, Ethiopia: Based on IPCC fifth assessment report (AR5) climate change scenarios. Hydrology, 7(4), 1–22. doi:10.3390/hydrology7040098.